Role of basin width variation in tectonic inversion: insight from analogue modelling and implications for the tectonic inversion of the Abanico Basin, 32°–34°S, Central Andes

P. JARA[1,2]*, J. LIKERMAN[3,4], D. WINOCUR[5], M. C. GHIGLIONE[3,5], E. O. CRISTALLINI[3,4], L. PINTO[2] & R. CHARRIER[2,6]

[1]*Departamento de Ingeniería en Minas, Facultad de Ingeniería, Universidad de Santiago, Chile*

[2]*Departamento de Geología, Facultad de Ciencias Físicas y Matemáticas, Universidad de Chile,Chile*

[3]*Consejo Nacional de Investigaciones Científicas y Técnicas (CONICET), Avda. Rivadavia 1917, CP C1033AAJ, Ciudad de Buenos Aires, Argentina*

[4]*Laboratorio de Modelado Geológico (LaMoGe), Instituto de Estudios Andinos Don Pablo Groeber. Universidad de Buenos Aires, Ciudad Universitaria, C1428EHA, Buenos Aires, Argentina*

[5]*Departamento de Ciencias Geológicas, Laboratorio de Tectónica Andina, Instituto de Estudios Andinos Don Pablo Groeber, Universidad de Buenos Aires, Buenos Aires, Argentina*

[6]*Escuela de Ciencias de la Tierra, Universidad Andres Bello, Santiago, Chile*

**Corresponding author (e-mail: pamela.jara@usach.cl)*

Abstract: We use analogue modelling to investigate the response of compressional deformation superimposed on an extensional basin with along-strike changes in width. Parameters described include extension and shortening distribution and directions, orientation of structures and degree of basin inversion. Two types of model are presented: in the first (Type I), an extensional basin is constructed with variable width (applying differential extension) and subsequently inverted by homogeneous shortening; in the second (Type II), an extensional basin with constant width is subsequently inverted by inhomogeneous shortening (differential compression). From our observations, we compare both types of model to structural patterns observed in some natural cases from the Central Andes. Both models generate oblique structures, but in the Type II model a significant rotation is characteristic. Our results suggest that in the Central Andes region between 32° and 33°S, the Abanico Basin may correspond to a basin of smaller area compared to the larger basin south of 33°S. Our Type I model further explains some patterns observed there, from which we conclude that the control exercised by the width of a pre-existing basin should be considered when interpreting the geological evolution of that area of the Andes.

The complexity of tectonic inversion systems involves a number of controlling factors such as orientation of pre-existing structures, reactivation angle and syntectonic sedimentation, among others. Rift zones associated with extensional regimes are generally controlled by the presence of lithospheric weaknesses or by previous fabrics of the upper-crust. Extensional development along rift basins may be heterogeneous and is generally characterized by along-axis segmentation in a series of single sub-basins with sedimentary and structural differences (Corti 2003). Furthermore, subsequent compressional phases may induce the reactivation of pre-existing normal faults and the inversion of these extensional systems. A large amount of new forming structures can be also generated, producing substantial changes with respect to the original extensional pattern, so different trending structures can coexist (Cooper & Williams 1989; Gillcrist *et al.* 1989; Coward *et al.* 1991; Turner & Williams 2004).

Changes in the structural trend of an arc-shaped orogen (map-view curve) can be attributed to various factors, including the architecture of the pre-deformational sedimentary basin, inversion of pre-existing extensional structures (Vergés & Muñoz 1990; Burbank *et al.* 1992), along-strike displacement gradients (e.g. Elliott 1976), interaction of a thrust belt with foreland obstacles or promontories, salients and recesses (oblique and lateral ramps) in the sole thrust (Macedo & Marshak 1999),

From: Sepúlveda, S. A., Giambiagi, L. B., Moreiras, S. M., Pinto, L., Tunik, M., Hoke, G. D. & Farías, M. (eds) *Geodynamic Processes in the Andes of Central Chile and Argentina*. Geological Society, London, Special Publications, **399**, http://dx.doi.org/10.1144/SP399.7

hinterland collision of an indenter (Ghiglione & Cristallini 2007; Reiter *et al.* 2011), interaction with strike-slip faults and warping of the downgoing (underthrust) plate (Marshak 2004), along-strike variations of the frictional properties of the décollement level (Cotton & Koyi 2000), rheological or thickness changes in the detached cover (Thomas 1990; Calassou *et al.* 1993; Corrado *et al.* 1998), lateral variations of thickness in the sedimentary wedge (Soto *et al.* 2002) and/or along-strike variations of syntectonic sedimentation and erosion rates (Nalpas *et al.* 1995; Dubois *et al.* 2002; Panien *et al.* 2005). Some curved orogens involve continental-scale rotation of segments of the fold–thrust belt and are called 'oroclines', assuming that the curve was due to the rotational bending of an originally straight orogeny (Carey 1958; Marshak 2004; Ghiglione & Cristallini 2007).

Analogue modelling is a powerful tool that helps interpret geodynamic environments, because it allows the simplification and investigation of isolated parameters of the studied processes. When scaled experiments are carried out (Hubbert 1937; Ramberg 1981; Weijermars & Schmeling 1986), the results can then be compared with natural examples. Previous analogue models study the mechanics and geometry of tectonic inversion (Koopman *et al.* 1987; McClay 1989; Buchanan & McClay 1991; Krantz 1991; Mitra & Islam 1994; Keller & McClay 1995; Brun & Nalpas 1996; Yamada & McClay 2003; Gartrell *et al.* 2005; Panien *et al.* 2005; Del Ventisette *et al.* 2006; Sandiford *et al.* 2006; Konstantinovskaya *et al.* 2007; Amilibia *et al.* 2008; Yagupsky *et al.* 2008; Pinto *et al.* 2010).

Our modelling is inspired by contributing to a better understanding of factors that control some latitudinal variation in strikes of structures and the evolution of the Central Andes. Experimental results are compared with the Eocene–Miocene Abanico Basin developed between *c.* 28° and 39°S (Charrier *et al.* 2002, 2007, and references therein), which has a history of extension followed by compression and inversion of previous structures. The complexity of the inversion process caused subsequent heterogeneous latitudinal deformation, which produces latitudinal changes in the style of deformation and strike of some structures (Jara *et al.* 2009; Jara & Charrier in press). Within the context of the Abanico Basin, the study region corresponds to the High Central Andean between 32° and 34°S. South of 33°S, many studies recognize that the Abanico Formation's volcanic rocks were deposited in an extensional basin over 50 km wide, with an approximately north–south orientation and high subsidence rates, with some depocentres reaching more than 3.5 km in depth (Charrier *et al.* 2002, 2007; Fock *et al.* 2005; Farías 2007; Farías *et al.* 2010). North of 33°S, new field-based data indicate that distal facies of this formation, which crop out in the eastern side of the Principal Andean Cordillera at this latitude, accumulated in a basin less than 10 km wide with an estimated thickness of *c.* 3.0–3.5 km (Jara & Charrier in press).

In order to study the influence of extensional basin width on subsequent superimposed compressive structures and their trend, two main types of model (I and II) were configured to study the effect of two principal variables: homogeneous shortening with variable basin width (Type I) and inhomogeneous shortening (differential) with a constant-width pre-existing basin (Type II). In both studies we distinguish whether or not the resulting structures are linked with positive inversion (Cooper *et al.* 1989; Coward 1994).

Analogue models

Strategy

Analogue modelling was carried out at the Laboratorio de Modelado Geológico (LaMoGe) at the Universidad de Buenos Aires to investigate the effects of inherited differential basin width on deformation patterns, such as plan view strike, number of structures and structural patterns during basin inversion. The selected experiments are representative of two possible tectonic configurations. In the Type I model, we investigate the influence of along-strike variations produced by differential extension in a wedge-shaped rift basin where extension increased from a pivot point, followed by homogeneous shortening in response to orthogonal convergence. In the Type II model, a homogeneous orthogonal extension was followed by a rotational convergence, where differential shortening increased from a pivot point.

In referring to the sectors of our experiments we will consider that a region affected by differential extension may develop main depocentres or sub-basins in a wider zone, whereas areas with less extension can generate isolated sub-basins in a narrow zone (Fig. 1a). During differential compressional tectonics, the most shortened region will generate greater uplift and compressional structures than the less shortened region (Fig. 1b). These conceptual models do not consider previous structural arrangements, but they are the starting point for our study of deformation width control in a tectonic inversion process.

Set-up and experimental procedure

The experiments were performed without boundaries in a platform of size 70 × 50 cm. Subtraction of edge effects in the final process allowed us to

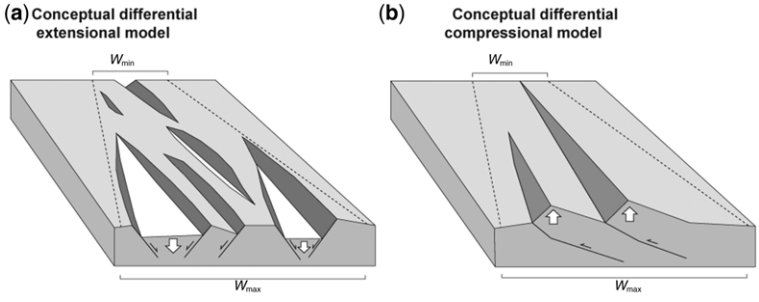

Fig. 1. Conceptual models of (**a**) differential extension and (**b**) differential compression. The vergence of structures is schematic and only referential. In both conceptual models there are no predeformation structures. The white arrows show the subsided (down) and uplifted (up) zones. The dotted lines correspond to the main deformation limits interpreted. W_{min} and W_{max} indicate the minimal and maximal width, respectively.

analyse a deformed sandbox of with dimensions of 55 × 40 × 3.5 cm (Fig. 2). The models were deformed by pulling/pushing a backstop attached to a mobile basal plate, generating a velocity discontinuity (VD) below the sandbox (Fig. 2a). The mobile basal plate produced extension along a basal silicon layer and was disconnected during compression, similarly to other experimental set-ups (Yagupsky *et al.* 2008; Likerman *et al.* 2013). In this way, compression was applied from the mobile wall, similar to a natural assembly, because compression through a mobile basal plate would generate structures rooted in the VD.

The backstops used in our experiments allow differential movements through a pivot point located at one end acting as a vertical axis of rotation (Fig. 2b). The backstop rotation was produced by pulling/pushing the free edge of the backstop connected to a worm screw driven by a stepmotor at a constant linear velocity of 4 cm/h in all models. The angular velocity imposed on the backstop was 4°/h, and can be considered constant throughout the experiment (for more details see Soto *et al.* 2006). A maximum backstop rotation of 10° was reached, for both extensional and compressional phases, equivalent to a maximum extension/shortening of 10 cm achieved in the area furthest from the pivot point, and progressively diminishing toward the pivot end where the deformation was null. For non-rotational deformation a maximum 10 cm shortening was achieved. Deformation phases applied to different sets (Type I and Type II models) of experiments are simplified in Fig. 3.

It is recognized that there is a minor strike-slip component in the model when generating rotational movement of the basal plate (extensional differential phase for the Type I model). This component was measured and is considered negligible in relation to the components perpendicular to the strike. In this study we focus only on the normal and reverse components.

Materials

Brittle layers are represented by well-sorted dry quartz sand with well-rounded grains (finer than

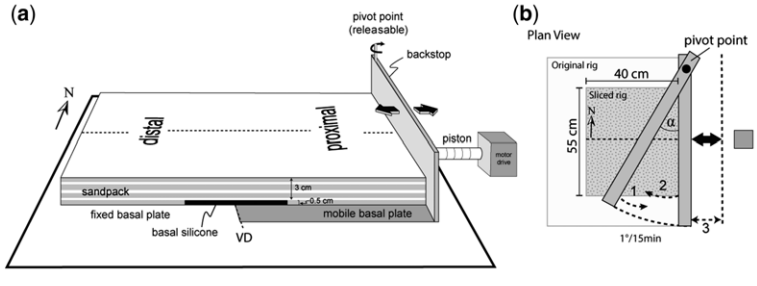

Fig. 2. (**a**) Model set-up and zones for the description of models. Proximal and distal are related to the distance to the backstop. (**b**) Plan view and different movements applied to the backstop: α, angle of backstop rotation; 1, differential extensional movement applying rotating backstop; 2, differential compressional movement applying rotating backstop; 3, homogeneous (orthogonal) movement of backstop by releasing the pivot.

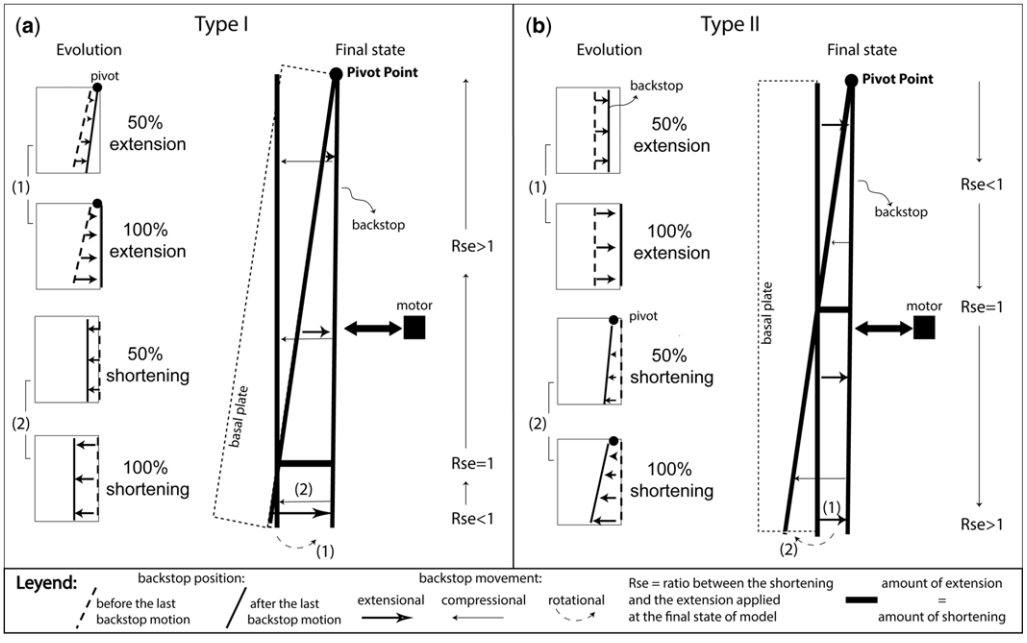

Fig. 3. Movement of the backstop schemes and percent extension and shortening during the evolution of the models, (**a**) Type I and (**b**) Type II, at different stages.

500 μm), with behaviour similar to that of the brittle upper-crustal rocks (Hubbert 1951). In such materials, frictional contacts between the grains result in a Mohr–Coulomb-type failure envelope, with small cohesion (<100 Pa) and an angle of internal friction close to 32.7° (Yagupsky *et al.* 2008), as measured with a modified Hubbert-type shear apparatus (Hubbert 1951). The material's density ρ is *c.* 1400 kg m^{-3} and the density ratio between the granular materials used and the rocks is $\rho^* \approx 0.5$. The stretching at the base of the brittle upper crust was modelled with a 0.5-cm-thick layer of SGM 36 polymer. SGM 36, a Newtonian viscous material manufactured by Dow Corning, has a density of 965 kg m^{-3} with an effective viscosity of 5×10^4 Pa s at room temperature (20 °C). A fine silicone layer (0.5 mm) was added above the VD. In these experiments the silicone does not simulate any character of the crust and has only a geometrical purpose (Brun & Nalpas 1996; Pinto *et al.* 2010), allowing the strain to be distributed and creating a wider deformation zone. The use of SGM 36 in analogue modelling is well documented (Weijermars 1986); it forms an analogue for materials with viscosities between 10^{18} and 10^{21} Pa s, which is sufficiently similar to those commonly used for high décollement viscosities (Van Keken *et al.* 1993; Weijermars *et al.* 1993). The models are thus broadly scaled to represent a strong natural décollement.

Scaling

To contrast analogue models with natural examples, the experiments required proper scaling of the model parameters (Hubbert 1937; Ramberg 1981). In the present experiments, the length ratio between model and nature was $L = 10^{-5}$ (so 1 cm in the model corresponds to *c.* 1 km in nature), and the gravity ratio between model and nature is $g^* = 1$, as both the prototype and the model are subject to the same gravitational acceleration. The corresponding stress ratio between model and nature is $\sigma^* = \rho^* g^* L^* \approx 6 \times 10^{-6}$. The scaling parameters for extension and compression are provided in Table 1.

Although the experimental set-up lacked the prerift brittle structures that may appear in nature, which can play an important role in the interaction and development of extensional structures (Sibson 1985; Huyghe & Mugnier 1992; Faccenna *et al.* 1995; Ranalli 2000), emphasis was placed on the interaction between rift structures and subsequent shortening.

Data collection and three-dimensional reconstruction of deformed models

A fixed high-resolution digital camera was used to photograph the top surface of the models at regular time intervals in order to study the time–space

Table 1. *Type I and Type II models' scaling parameters in both extensional and compressional phases*

	λ (μm)	g (m s^{-2})	ρ (kg m^{-3})	μ (Pa s)	V (m s^{-1})	σ (Pa)	ε (s^{-1})
Nature	1000	9.81	2300	1.8×10^{21}	5×10^{-13}	2.2×10^{7}	Oct 14
Model	0.01	9.81	1400	5×10^{4}	1.1×10^{-5}	1.4×10^{2}	2.2×10^{-3}
Model/nature(*)	10 May	1	0.6	2.7×10^{-17}	2.2×10^{7}	6×10^{-6}	2.2×10^{11}

evolution of the structures. At the end of the experiments, dry sand was sieved onto the model's surface to preserve the final topography. To reconstruct a three-dimensional geometry, the models were impregnated with hot gelatin solution and, once cooled and slightly hardened, were sliced (*c.* 5 mm) perpendicular to the principal structure's trend. In this way, internal structural arrangements of the final state of the models could be analysed.

The top surfaces of the models were scanned at regular time intervals with a laser with *c.* 0.135 mm of vertical accuracy. The data obtained were processed to remove spurious data. Subsidence of the top surface was calculated from the incremental difference between successive gridded data. In the shortening phase, incremental topographic maps were obtained, revealing the development of contractional structures. Model evolution was visualized by measuring diagnostic parameters along strike positions representative of wide and narrow deformed sectors close to (north) or away from (south) the pivot (Fig. 2). This methodology, together with photography, allowed a more rigorous and detailed interpretation of the development of the structures.

Synrift sand thickness was used to identify inverted faults. Synrift sand deposits on the hanging wall of normal faults are thicker than on the equivalent footwall, so inversion will show thicker packages of synrift lifted on the hanging wall of positively inverted faults. Moreover, the presence of faults planes with normal and inverse movement was used to identify incomplete reversal movement.

Statistical fault analysis

In the final stages, fault traces were mapped over the plan view. Fault traces intercepted by a 0.5 cm-wide belt in two representative sections were analysed quantitatively in terms of length and azimuth distribution. To analyse the fault's azimuth distribution, the polyline features used to map the fault traces were transformed into tip-to-tip lines (Agostini *et al.* 2011). The azimuth data were weighted for the length of the corresponding fault. The weighting factor for each fault was the ratio between its length and the minimum fault length intercepting the belt, such that long faults have higher ratios than short ones. The frequency of the azimuth of a tip-to-tip fault is directly related to this ratio; the longer the fault the higher its frequency. This type of fault pattern outcome has often been coupled with analogue models, providing the basis for a well-established approach that has been successfully applied to the determination of rift kinematics in oblique extension settings (Dauteuil & Brun 1996) and continental rifts (Brun & Tron 1993; Bonini *et al.* 1997).

Analogue modelling results

Six experiments were performed to test the control that axial width variation in an extensional basin has on the strike of subsequent inversion structures. The structural configuration obtained was relatively similar for each type of experiment. Because of limited space, only two are described here, one for each type. In order to simplify the description of the results, in the following we will use a series of acronyms to refer to the different sectors of both models (Fig. 2). Sequential photographs of the tops of the three-dimensional (3D) models during the evolution of the experiment, together with isopach maps highlighting the differential subsidence or uplift between each stage, are presented. Additionally, internal structure interpretation is shown in serial vertical sections for the end of this phase. For descriptive purposes, the terms proximal and distal are used relative to the advancing moving wall (Fig. 2a), and forethrusts for those faults dipping towards the moving wall and backthrusts for those dipping in the opposite direction.

In the Type I model, maximum extension (100% extension) was reached after applying 10 cm of movement to the backstop, as measured on the zone further away from the pivot (Fig. 3). During the ensuing compressional phase the mobile wall was released from the pivot and was moved until completing 10 cm of homogeneous compression (100% shortening) perpendicular to the last extensional movement, producing total inversion of the extensional basin (Fig. 3a). In the final state of the Type I model there is a variable amount of extension and shortening for a given point, so we have included a factor ('Rse') relating the amount of applied shortening to the amount of previous

extension in sections at different distances from the pivot (Fig. 3).

In Type II models, extension was homogeneous in applying a 5 cm motion to the backstop (100% extension, Fig. 3b). The result was a 15-cm-wide basin, a width similar to that of the central zone of the basin in the Type I model. During the compressional phase, the pivot was connected to achieve a differential shortening. The region further away from the pivot reached a maximum 10 cm, or 100% shortening (Fig. 3b). As with the Type I model, in the final stage we use the same factor ('Rse') to compare the amount of extension and shortening applied in different sections according to their distance from the pivot (Fig. 3).

Type I: Along-strike width variation of basin and subsequent inversion

Extensional phase evolution. The initial stages of the extensional phase (Fig. 4a) produced a symmetric basin defined by two sets of normal faults with opposite dips. Subsequently, with 25% extension, the deformation concentrated in a direction parallel to the backstop. The isopach map (Fig. 4a) highlights the differential subsidence between the non-deformation stage and the 100% extension after every 25% displacement of the backstop; deepening of the basin shows progressively more activity and a large basin width focused on the southern zone.

From 25% to 50% of extension, structures in the proximal zone generated deepening of the basin, mainly in the southern zone (Fig. 4a). Subsequently, subsidence ends in the middle part of the model, generating some horsts between sub-basins or graben (see Fig. 4c and non-coloured areas within the main basin in Fig. 4a). The high activity (subsidence and active faults) is seen mainly in the southern and proximal zones. This becomes most evident between 50% and 75% of extensional displacement (Fig. 4a).

Between 50% and 75% extension (Fig. 4a), the activity of the distal zone of the main basin is almost null, while in the proximal zone the basin is active and sub-basins coexist (note subsidence symbology colours in Fig. 4a). Sub-basins in the northern zone are oriented approximately north–south, while in the southern proximal zone they have a general approximately N10°E strike (although one reaches a maximum of 30° obliquity) (Fig. 4a).

Extension ended at 10 cm (100% extension) of displacement in the southern zone, and in this last stage the distal basin zone is reactivated (Fig. 4a) but with much lower activity compared to the proximal zone, which preserves the features described above, but with further deepening of depocentres in the basin (note subsidence symbology colours in Fig. 4a).

Extensional phase final state. The proximal and distal limits of the basin have oblique (<15°) orientations, which generate its triangular shape, but its main depocentres have a north–south orientation (Fig. 4a). In the northern zone, two graben separated by a horst were generated, both bounded by normal faults with opposing dips (Fig. 4c, profile I). Deformation and faulting were localized above the VD characterized by a set of normal faults with dipping angles from 50° to 65° (Fig. 4c, profiles I–II), but towards the southern zone (Fig. 4c, profile III) some normal faults are very flat with dips up to 20°. The deepest sub-basin occurs from the middle of the model to the southern zone (Fig. 5) and is mainly concentrated in the proximal zone of the basin, as seen in the plan view evolution (Fig. 4a) and in the cross-sections of the final result (Fig. 4c).

Compressional phase evolution. An important topographic increase developed homogeneously along the entire model, mainly in the internal region (in the location of the previous extensional basin) and in the proximal zone, as shown by the isopach maps highlighting the differential uplift between each stage (Fig. 4b). With 25% of shortening, there is uplift in the proximal region of the northern zone quite near the mobile wall and an important uplift at the proximal inherited graben in the southern zone (Fig. 4b). Structures that limit these uplifted areas have approximately north–south strike in the southern zone, and approximately N10°W in the proximal zone in the north (Fig. 4b).

Between 25% and 50% of shortening, deformation is mainly concentrated in north–south backthrusts in the central part of the extensional basin (Fig. 4a,b). The activity of these north–south backthrusts decreases towards the north where shortening is transferred to the proximal zone (Fig. 4b). In this region away from the pre-existing basin, the main forethrust with N10°W strike is better developed, generating large uplift (note the increase in topography bordering the structure in Fig. 4b). In the northern zone, uplift also occurs in the inherited basin generated by approximately north–south to N10°E strike backthrusts. Towards the southern zone, shortening is mostly concentrated in the region previously occupied by the basin, although some rising is generated out of the basin, mainly in the proximal zone (Fig. 4b).

With 75% of accumulated shortening, deformation concentrates in two major regions. In the northern region it is concentrated in the N10°W structure, leading to an important rising of the proximal zone, while in the southern region the main structures correspond to approximately

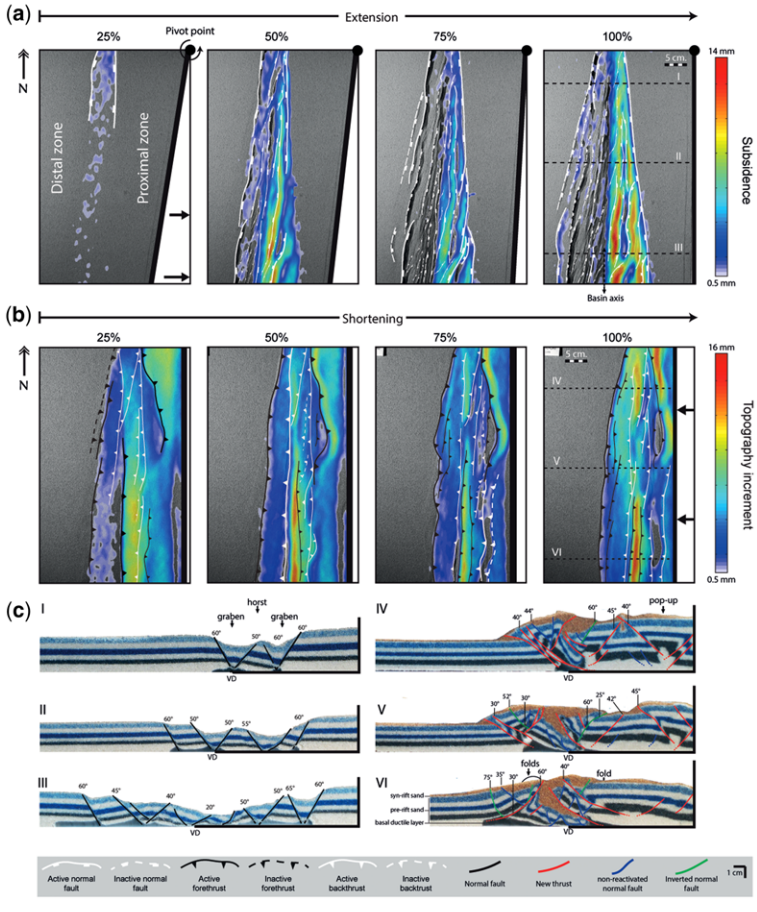

Fig. 4. Type I model evolution. (**a**) Extensional phase: active subsidence at different extension percentages. (**b**) Compressional phase: active topography increment at different shortening percentages. (**c**) I, II, II: profiles of the final result after differential extension. IV, V, VI: profiles of the final result after homogeneous shortening.

north–south strike forethrusts and backthrusts, bounding the uplifted proximal area of the inherited basin. Towards the distal zone, part of the shortening occurs in the inherited basin, as indicated by the 'triangular' shape of the uplift in the northern zone. In the northern zone there is also activity (topographic increase in Fig. 4b) produced by backthrusts in the proximal area (centre of the inherited basin), but this is lower than that in the south.

Between 75% and the last stage of shortening (Fig. 4b), the features described above are preserved, but the activity of the main approximately north–south strike structure (topographic increase at the centre of the inherited basin, Fig. 4b) becomes heterogeneous between north and south. The central portion of this north–south structure is completely inactivated at *c.* 90% of shortening, while in the northern zone this structure is reactivated between 90% and 100% of shortening. The oblique N10°W structure in the northern zone maintains its activity and generates increasing uplift throughout the course of the experiment (Fig. 4b).

Compressional phase final state. The final state (Fig. 4c, profiles IV, V and VI) shows that (1) faults inherited from the extensional stage have a heterogeneous behaviour (some were not reactivated and others were reactivated), (2) the southern zone has a greater density of normal faults, some preserved within folds of large amplitude that mainly concentrate the shortening in this region (Fig. 4c, profile VI), and (3) towards the northern zone a pop-up structure (uplifted area bordered by two new opposite dipping thrusts) of smaller amplitude and increasing uplift (Fig. 4c, profile IV)

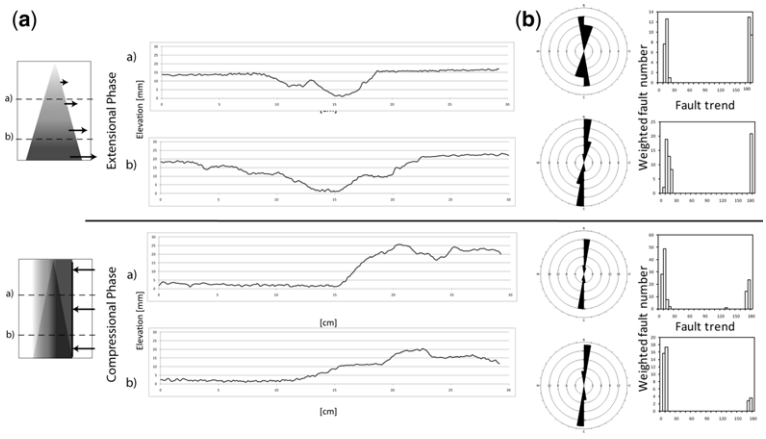

Fig. 5. (**a**) Topography of the final stages of the Type I model in the northern and southern zones. (**b**) Rose diagram and weighted fault number trend for the Type I model extensive and compressive end stage.

absorbs part of the shortening in the proximal zone where the basin was narrowest. The major topographic increase (elevation) developed along the entire model mainly in the proximal region and mostly in the northern zone (Fig. 5).

In the northern zone, compressive structures have an oblique strike in both the proximal and distal zones, while inactive normal or inverted normal faults have an approximately north–south orientation (Fig. 4) at the centre of the active zone (evidenced by a topographic increment).

Type II: Homogeneous extension and subsequent differential compression

Extensional phase evolution. Elongated north–south basins were generated (Fig. 6a). Distal to proximal migration of the deformation occurs, while the main activity (see the subsidence maps in Fig. 6a) moves towards the proximal zone at the centre of the basin (Fig. 6a). Normal faults dip towards the basin's centre. In some places, sub-basins are separated by horsts (note uncoloured areas with no subsidence between two adjacent normal faults dipping opposite in Fig. 6a). With more than 75% of extensional displacement, normal faults located in the distal zone became inactive. This did not occur on the basin's axis, above the VD, where the major activity was concentrated.

The extension ended at 5 cm of displacement (100% extension in Fig. 6a). At this last stage, the development of normal faulting along the whole model was emphasized, with approximately north–south strikes and the development of relay ramps between the extensional structures (note areas of lower subsidence between two normal faults displaced in the east–west direction in Fig 6a). Intrarift normal faults grew closely spaced and the rift border faults are well defined.

Extensional phase final state. After applying 5 cm of extension (100%), a 15 cm-wide basin was formed (Fig. 7a) that has a similar structural pattern to the central profile of the basin of the Type I model (Fig. 4), but with near north–south strike (Fig. 7b). The basin is formed by sub-basins, with the central region deeper than the edges (Figs 6c & 7a). The basin is relatively homogeneous along the course, with graben limited by normal faults dipping between *c.* 50° and 70° (Fig. 6c). In the centre of the basin, the deepest area presents low-angle normal faults, similar to those observed in profile III at the extensional phase of the Type I model (Fig. 4c). Its general structure can also be observed in the less deformed profile in the compressive stage of the Type II model, which shows that all faults are rooted in the ductile layer (Fig. 6c, profile IV).

Compressional phase evolution. During the initial shortening phase (0–25% shortening) the deformation is concentrated mainly in the southern zone (Fig. 6b), between the distal boundary of the pre-existent basin and the area proximal to the backstop. Uplift in the northern zone is less than in the southern zone and it concentrates in the proximal region, as shown in the isopach maps in Fig. 6b. With increasing shortening (50% in Fig. 6b) the elevated region expanded; some deformation is transferred towards the northern distal zone, but within the limits of the pre-existent basin.

From 75% to 100% shortening (Fig. 6b) it is clear that in the distal zone of the model the structures exhibit an approximately north–south strike, similar to the structures of the pre-existent basin,

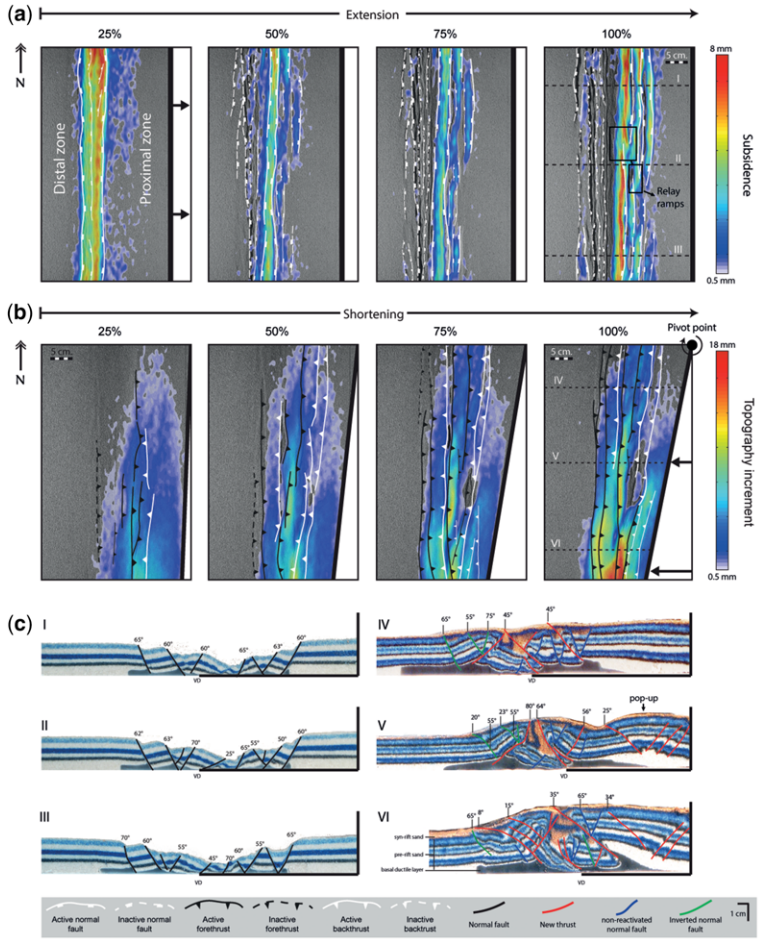

Fig. 6. Type II model evolution. (**a**) Extensional phase: active subsidence at different extension percentages. (**b**) Compressional phase: active topography increment at different shortening percentages. (**c**) I, II, II: profiles of the final result after homogeneous extension. IV, V, VI: profiles of the final result after differential shortening.

whereas structures in the proximal zone occur with an obliquity similar to that of the mobile wall, with a N10°E maximum strike. Note that this obliquity occurs in backthrusts that were already generated before 75% shortening, which means that they have been rotated and are not new oblique structures.

The deformed area does not vary significantly during the evolution of the model, but the amount of uplift increases from the beginning of compression until it reaches 100% (Fig. 6b), indicating that the region is progressively uplifted and rotated until it absorbs 100% of the applied shortening.

Compressional phase final state. In the northern zone (Fig. 6c, profile IV), a principal forethrust absorbs part of the deformation uplifting the proximal zone above the pre-existent basin, while a backthrust in the distal zone produces the same effect with opposite vergence. It is possible to follow this structures to the profiles of the southern zone (Fig. 6c, profiles V and VI), given its approximately north–south strike. Some normal faults were reactivated; however, most of the normal faults were not reactivated. It is remarkable how the number of thrusts increased along the strike with increasing shortening, while their spacing decreased (Fig. 6c). These structures generated greater rise into the southern zone compared to the north (compressional phase in Fig. 7).

In profile IV (Fig. 6c), all deformation is concentrated in the area occupied by the previous basin. The proximal forethrust preserves some non-reactivated normal faults in its hanging wall, while

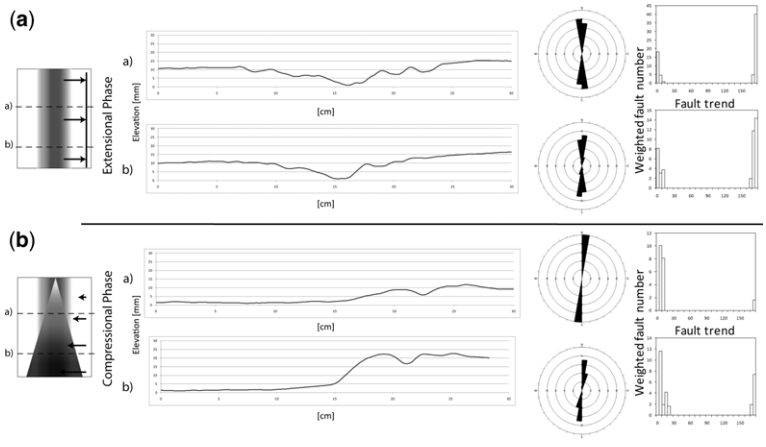

Fig. 7. (**a**) Topography of the final stages of the Type I model in the northern and southern zones. (**b**) Rose diagram and weighted fault number trend for the Type I model extensive and compressive end stages.

some inverted normal faults are recognized in the hanging wall of the distal backthrust (Fig. 6c, profile IV). Most of the normal structures are preserved non-reactivated at the proximal zone, where they generated the major subsidence in the previous phase.

In the centre of the model (Fig. 6c, profile V), where the amount of shortening was equal to the amount of applied extension, the proximal forethrust and the distal backthrust into the inherited basin had greater activity and produced two opposite verging folds, closing the basin towards its axis. An anticline fold, consisting of a pop-up structure, was created out of the basin in the proximal region (Fig. 6c, profile V). Towards the south, this anticline fold rises as a result of the activity of the forethrust mentioned above (Fig. 6c, profile VI), generating greater rise into the southern compared to the northern zone (compressional phase in Fig. 7a). Throughout the region, several normal faults are preserved, while some normal faults dipping towards the proximal zone are slightly reactivated.

Discussion

Summary and interpretation of results

It has been reported that initially high-angle normal faults may rotate to gentler dips (more favourable for reactivation) during extension through 'domino' rotation of successive normal fault sets (Jackson & McKenzie 1983; McClay *et al.* 1989; Buchanan & McClay 1991; Knott *et al.* 1995; Mandal & Chattopadhyay 1995; Del Ventisette *et al.* 2006; Bonini *et al.* 2012). In our models, normal faults distinguished by their low dip angle occur in the central part of the most extended zone in the Type I model (southern zone) and at the centre of the basin of the Type II model. From the observation of profiles in plan evolution, and 3D building blocks shedding light on the north–south continuity of some structures, we interpreted a 'domino' block rotation mechanism (Buchanan & McClay 1992; McClay & Buchanan 1992; Mitra 1993) of initially steep normal faults formed with *c.* 60° dip in the early stages of extension to minor inclination normal faults at the final stages, presenting angles even less than 20°.

Moreover, the compression in the southern zone of the Type I model is highly concentrated inside the basin (Fig. 8a), so reverse faults are formed mainly within the limits of the previous extensional basin, while in the northern zone, where the pre-existing basin was narrow, new compressive structures developed out of the limits of the basin (Figs 8a & 9). Positive inversion is concentrated in the southern zone of the Type I model, where pre-existing faults prone to positive reactivation due to the low angle are located (Figs 8a & 9).

In both types of model proposed for this study, some normal faults are preserved after inversion of the basin (Figs 4c, 6c & 9). Reactivated faults generally have high dipping angles of 50°–60° (Fig. 9), whereas in the central profiles of both models (profile V in Figs 4 & 6), the dipping of reactivated normal faults decreases toward the surface. Similarly, Likerman *et al.* (2013) and Konstantinovskaya *et al.* (2007) noted that, for asymmetric rifts, reactivated normal faults rotated to gentler dips when cutting off to the surface.

Additionally, in the region where the rift basin was poorly developed (northern zone in the Type I model), the deformation is accommodated by

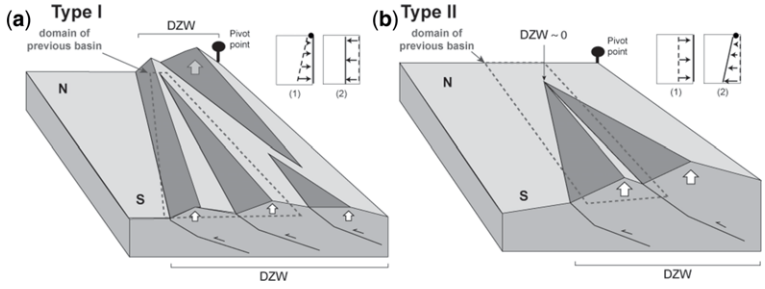

Fig. 8. Conceptual models of main features of the final results of (**a**) the Type I model and (**b**) the Type II model. The vergence of structures is schematic and only referential. White arrows show the uplifted zones. DZW, deformational zone width during compression. (1) and (2) correspond to the extensional and compressional phases respectively.

structures that are capable of absorbing large amounts of shortening by raising a narrower area outside the rift basin (Figs 5 & 8a). This process causes the main forethrust, which generates this higher rise in this narrow region, to have an oblique strike (Fig. 4a) to connect with the wider area (south), where it generates a minor uplift area closest (proximal) to the backstop (Figs 8a & 9).

In the Type II model, compression by a rotating pivot generated a differential deformation zone. Faults and folding were concentrated in the area of maximum shortening (southern zone in Figs 8b & 9). The deformational plan view sequence and the structural pattern of the Type II model (Fig. 6b) have some similarities with compressional rotational models that do not involve the basin inversion process (Soto *et al.* 2006), because both have a progression that starts in the most compressed region, and the rotation is in the same direction as the rotation axis of the backstop. Similar to the Type II model (Figs 8b & 9), Ghiglione & Cristallini (2007) showed that rotation of a rigid indenter against a soft sedimentary cover produces a strong variation in orogenic shortening and width of the thrust belt along the strike of the pivoted edge. Deformation in the southern zone of the Type II model is concentrated in new thrusts, some normal reactivated faults and low wavelength folds (Fig. 9). In the northern zone there is little shortening and therefore most normal faults are preserved (Fig. 9). As compression progresses, deformation in the southern zone produces the rotation of structures (Fig. 6) and closing of the basin through main folds. Distal structures develop parallel to the basin and proximal thrust gradually turns in a more oblique direction (Fig. 6b), parallel to the shortening vector. In the more compressed region we can recognize some similarities with complex inversion models described in previous papers, such as decapitating early normal faults, shortcuts and buttressing (Coward *et al.* 1991; Scisciani 2009; Bonini *et al.* 2012).

Figures 5, 7, 8 and 9 summarize some of the characteristics of the developed models. The Type I model presents many normal structures in the southern zone and fewer in the northern zone, as expected (Fig. 5b). The principal structures are north–south oriented, but some structures show a direction linked to the imposed edges of the silicone basal layer, which forced the direction of the basin limits. During compression, the oblique NNW direction is not directly linked with the limits of the basal silicone; this is made evident because the main forethrust in the northern zone is not generated from the previous proximal limit of the basin, but far closer to the mobile wall (Figs 8 & 9). This NNW orientation of the proximal structures is interpreted as being produced by the greater uplift of the northern compared to the southern zone, which is the result after compressing both regions equally, but with different pre-existing basin widths.

In the Type II model (Fig. 7), a similar number of normal faults are created in the northern and southern zones, with a trend very close to north–south. Compressing this model produces fewer structures in the northern zone than in the Type I model (Fig. 9).

Our modelling technique included complete filling of the basin before inversion. Sediment load makes difficult or delays the reactivation of previous normal faults (Nalpas & Brun 1993; Brun & Nalpas 1996; Dubois *et al.* 2002; Panien *et al.* 2005; Del Ventisette *et al.* 2006; Pinto *et al.* 2010), while in models with load inside and outside the basin, reactivation is facilitated, allowing the interpretation that the dominant factor in this case is the relative difference in load (Pinto *et al.* 2010). In our models, the largest load difference occurs where the basin is deeper and wider, so we expect the reactivation to be difficult during inversion tectonics in these sectors. This is consistent, because, regardless of the width of the basin, inverted normal faults are generally located near the edges of the pre-existing basin (Fig. 9), where the filling (synrift) is thinner.

It is worth noting one important difference between the models mentioned above and ours. In our Type I models the greater width of the basin means that shortening occurs inside it, while in other models (Pinto *et al.* 2010), an increase in sediment load generates further development of thrust faults outside the basin, similar to what occurred in our filled narrow basin (Fig. 9). Although the sedimentary basin is greater in our wide basin than in our narrow basin, the amount of shortening is equal in both areas, leading to the ratio (Rse, Fig. 3) between the amount of shortening and the amount of extension (and the resulting basin width difference) to be the predominant factor in this case.

As the methodology used in the Type I models allowed extensional structures to be generated with the same strike in both wide and narrow basin areas (approximately north–south faults and basin edges with equal obliquity across the region), the orientation of these structures is not a predominant factor in discerning between reactivated faults among narrower and widest basin zones (Fig. 9).

At stages with differential deformation (rotating the pivot), a maximum of 10° of obliquity was applied to the mobile wall. This generated, for the Type I model, extensional structure strikes between 0° and 15°, leading to the subsequent applied direction of principal compressive stress (perpendicular to the main direction of the extensional basin) being inefficient for reactivation. Analogue model experiments showed that, without a change in the inclinaton of the previously formed normal structures to gentler dips, an optimum angle close to 15° between the direction of extension and compression is necessary to generate subsequent reversal of high-angle faults (Brun & Nalpas 1996). We obtained considerably higher angles between the compressive and extensive strain axes, and there is reactivation of structures in our models. We think this might be caused by flattening of some normal faults before compression.

The Type II models have a similar relation: the direction of compressive stress rotates together with backstop rotation (0–10°), so the angle between the two principal stresses is never as close

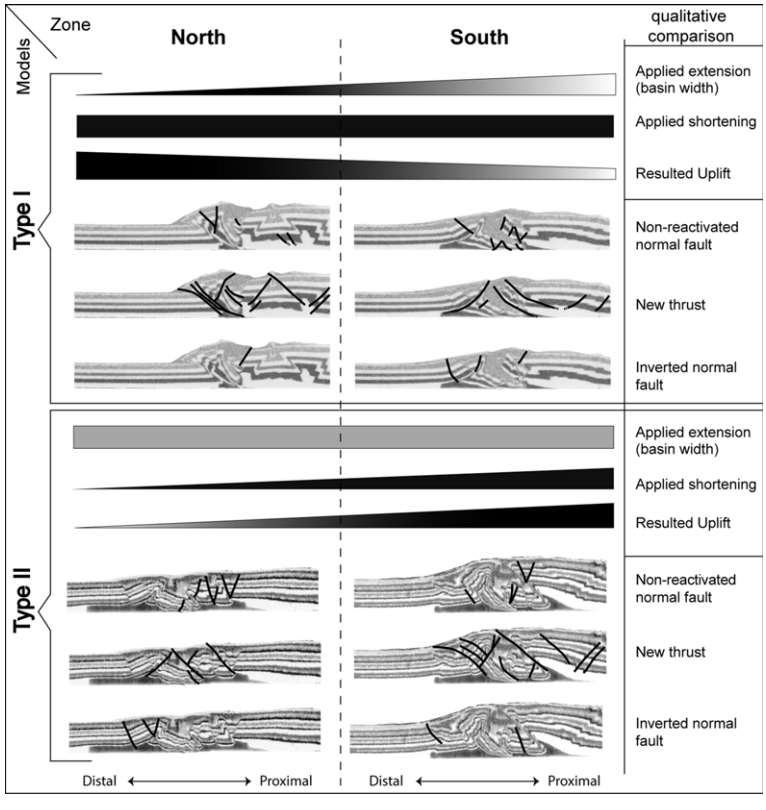

Fig. 9. Comparative chart of the main observed features in the final state in the northern and southern zones of the developed Type I and Type II models.

to 15°, and not enough to generate an efficient inversion process.

The north–south direction is a preferred orientation for major structures in extensional deformation phases of our models. However, in the Type I model this orientation is preferential for the major depocentres or sub-basins, whereas in the Type II model all extensional structures had this orientation prior to the shortening phase, and the obliquity of later structures is generated by the rotational movement of the pivot. Summarizing, the Type II model can explain the development of oblique structures, but it needs an important rotation. In the Type I model, latitudinal difference between uplift and width of the deformation zone play an important role in the obliquity of compressive structures.

The main results of our model are as follows:

(1) The preservation of non-reactivated normal faults, and positive inversion and generation of new compressive oblique structures, occur in both types of model.
(2) A significant rotation is required to generate obliquity of structures in models with no difference in the width of the pre-existing basin, as well as subsequent differential compression (Type II).
(3) In the Type I model, the obliquity of structures is generated due to a different width along the pre-existing basin.
(4) The northern zone in the Type I model and the southern zone in the Type II model are the areas that predominantly exhibit compressive structures (Fig. 9), but in the Type I model they are concentrated in a narrower and raised region due to the absence of a pre-existing wide basin.

Comparison with inverted natural basins

The elongated Abanico Basin, located in the Principal Cordillera of the Central Andes (Fig. 10a), presents significant latitudinal variations in the distribution and width of the Cenozoic outcrops in the strike of the major structures of the eastern Principal Cordillera, and the presence or absence of tectonic inversion structures, those that can be observed in latitudinal profiles (Jara *et al.* 2009; Godoy 2011, 2012). There is an observed south to north decrease in width of the Abanico Formation between 32°S and 33°S (Fig. 10c, d), which may correspond to an original extensional setting or to a subsequent narrowing due to a northward increased in shortening (Jara *et al.* 2009). In this comparison we will focus on the major structural features (strike of principal structures) and width of the deformational zone and outcrop of affected deposits (Fig. 11) in order to interpret the origin of the latitudinal changes based on the results of both developed models. Together with a comparison with the applied models, a brief background that will allow us to interpret the origin of these main features is further discussed below.

The Abanico Formation (Fig. 10) is represented by a set of volcanic-sedimentary rocks 3500 m thick (Thiele 1980; Fock 2005; Charrier *et al.* 2007; Rauld 2011), interpreted to have been deposited in an intra-arc extensional basin with active volcanism during the Late Eocene to Early Miocene, and tectonically inverted between *c.* 21 and *c.* 16 Ma (see Charrier *et al.* 2007, and references therein) and exposed in the Principal Cordillera of central Chile from 33° to 36°S (Aguirre 1960; Klohn 1960; González & Vergara 1962; Charrier 1973; Vergara & Drake 1979; Thiele 1980). Two stages are distinguished in the evolution of this basin: (1) a Late Eocene to Early Miocene extensional stage, where thick deposits of lava, volcaniclastics and minor sediments accumulated, and (2) an Early to Middle Miocene (Charrier *et al.* 2002, 2007, 2009) compressional stage. During this second stage, the Abanico Basin would have undergone partial tectonic inversion, probably contemporaneous with uninterrupted volcanism and accumulation of material included in the Farellones Formation (Middle–Late Miocene) (Charrier *et al.* 2002, 2005, 2007; Fock 2005; Fock *et al.* 2006; Pinto *et al.* 2010; Muñoz *et al.* in press). Charrier *et al.* (2005) showed evidence for the presence of the Abanico extensional basin from at least 33° and 36°S, and suggest its probable continuity north of 31°S and south of 37°S (Fig. 10a).

New data indicate that, between 32° and 32°30′S, and near the 'Las Llaretas' river (Figs 10b & 12), Oligocene–Miocene rocks are deformed by approximately north–south trending structures in the easternmost sector of the Principal Andean Cordillera (Jara & Charrier in press). These rocks are located in areas where intense compressional deformation is superimposed on Late Oligocene depocentres bounded by approximately north–south normal faults that were later inverted. Some of these faults had extensional movements accommodating clastic deposits at least 21 Ma ago. Post-18 Ma, these structures were reversed, deforming clastic deposits of the basin (synrift) as well as overlying discordant accumulated cenozoic strata (post-rift) (Fig. 12).

At these latitudes (32°–32°30′S), eastern units of the Abanico and Farellones formations are affected by NNW-oriented out-of-sequence faults of the La Ramada fold-and-thrust belt (Fig. 11). Although the La Ramada fold-and-thrust belt has been described as a thick-skinned fold-and-thrust belt (Mosquera 1990; Zapata 1990; Cristallini & Cangini 1993; Cristallini *et al.* 1994; Alvarez

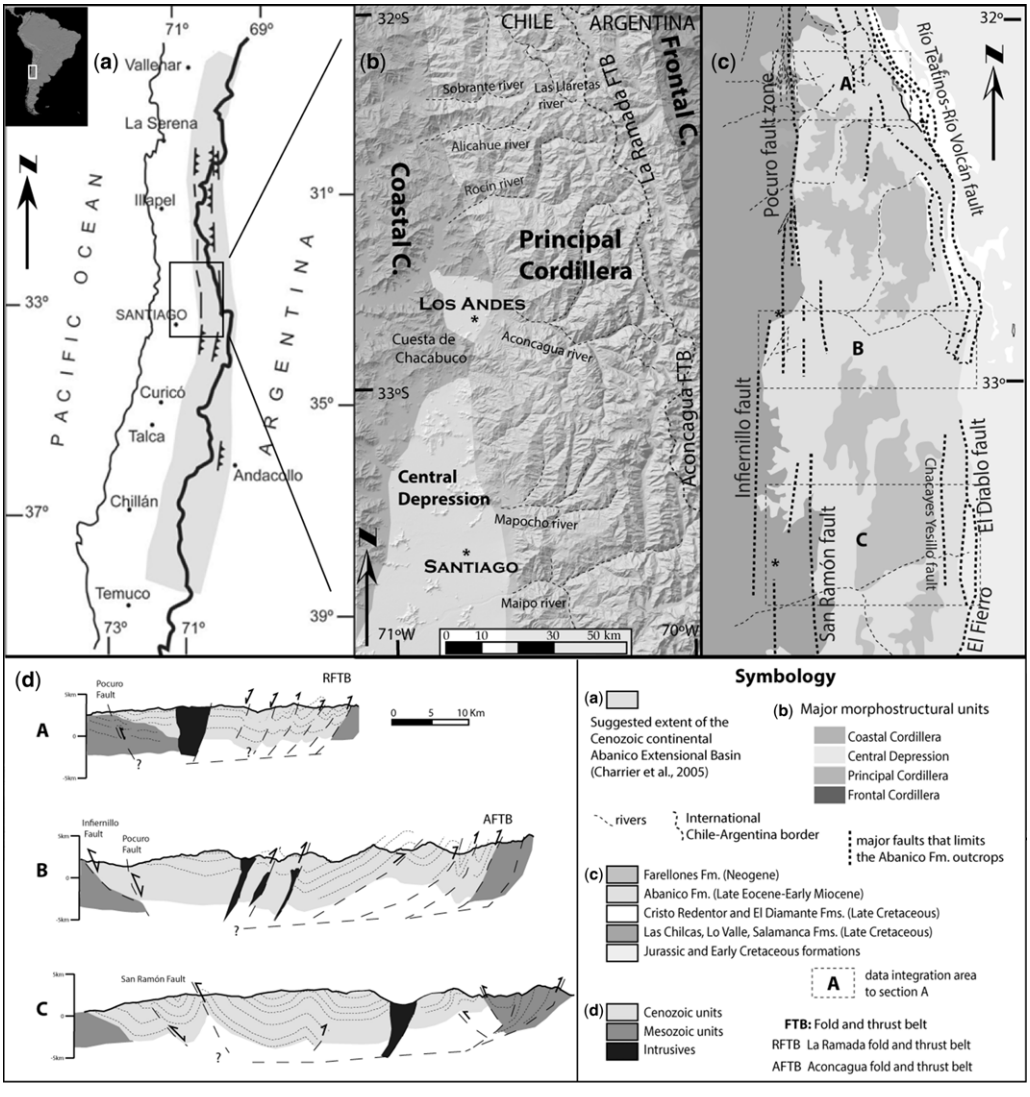

Fig. 10. (**a**) Tentative suggested extent of the Cenozoic continental Abanico extensional basin along the Principal Cordillera (Charrier *et al.* 2005). (**b**) Major morphostructural units and localities at *c.* 32°–34°S. (**c**) Simplified geological and major structures that limit the Abanico Formation outcrops. (**d**) Schematic sections of deformed units of the Principal Cordillera in central Chile between *c.* 32° and 34°S.

et al. 1995; Pérez 1995; Cristallini 1996), the out-of-sequence structures in this region only affect Cenozoic levels (Jara & Charrier in press).

The eastern NNW-strike structural pattern in this region has been explained previously (Rivera & Yáñez 2007) as a result of an originally segmented basin with sub-basins bounded by oblique structures controlled by heterogeneities of the Triassic–Jurassic basement under the Mesozoic to Cenozoic cover. The influence of Triassic–Jurassic rift structures on the deformation style in Andean structures has been studied from various points of view by several authors (Giambiagi *et al.* 2003*a*, *b*, 2005, 2009*a*, *b*; Yagupsky *et al.* 2008). In particular, the structural control that these basement structures exerted on Tertiary tectonic inversion has been studied and recognized in the fold-and-thrust belt of La Ramada (RFTB), Aconcagua (AFTB) and Malargüe (MFTB) (Cristallini & Cangini 1993; Cristallini *et al.* 1994; Maceda & Figueroa 1995; Giambiagi & Ramos 2002; Giambiagi *et al.* 2005; Yagupsky *et al.* 2008). Hovewer, the mainly NNW orientation of the main

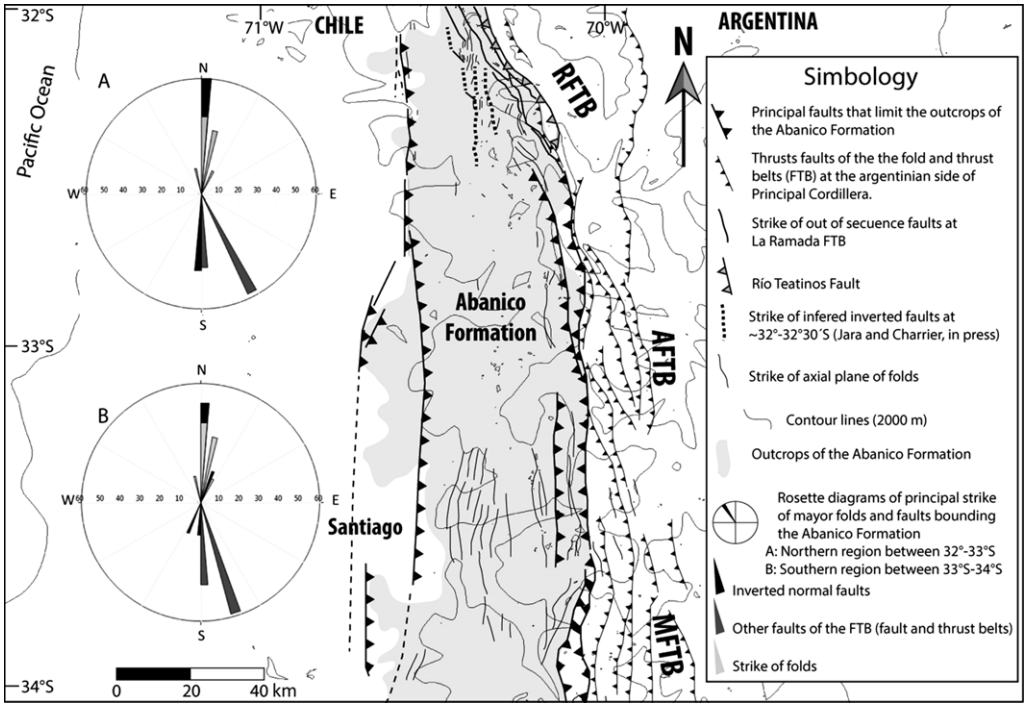

Fig. 11. Abanico Formation outcrops and major structure trends along the Principal Cordillera between *c.* 32° and 34°S.

structures in the eastern Principal Cordillera in this region would be associated with Tertiary deformation and not necessarily with the Abanico Basin original boundaries, or even older basins. We propose a not previously considered control, variable basin width, to explain in part some of the characteristics of this region, including distribution and width of the Cenozoic outcrops, the strike of the major structures and the presence or absence of tectonic inversion structures.

Cristallini (1996) indicates that the structural evolution of the La Ramada fold-and-thrust belt would have begun around 19–20 Ma ago, before flat-slab development in this region. The first stage of this structural evolution developed the first folding and faulting in Argentinian territory, and the first rise of the Principal Cordillera in the Chile–Argentina bordering region, controlled by approximately north–south preferential trending faults (Cristallini 1996). At this stage, in the eastern sector of the Principal Cordillera between 32° and 33°S (Jara & Charrier in press), some of the normal faults that previously controlled the accumulation of distal deposits of the Abanico Formation were reversed (Fig. 13).

The subsequent stage of deformation in the La Ramada fold-and-thrust belt, developed between *c.* 14 and 12.7 Ma (Pérez 1996), was controlled by the reactivation and inversion of ancient Triassic rift normal faults, which have an essentially NNW strike and raised basement blocks (Cristallini 1996). Basement uplift by high-angle reverse faults produced a 'sticking point' in the foreland propagation of the thrust belt, responsible for the third stage of deformation characterized by thin-skinned NNW out-of-sequence thrusts developed in the westernmost sector of La Ramada fold-and-thrust belt (Cristallini & Ramos 2000). The NNW-trending faults in the eastern part of the Principal Cordillera between 32° and 33°S, in Chilean territory, correspond to the westernmost of these out-of-sequence structures and are controlled by a shallower detachment level than those that would have inverted the basement of the La Ramada fold-and-thrust belt (Cristallini 1996; Cristallini & Ramos 2000; Ramos 2006).

In the southern region (south of 33°S), the structures are generally north–south oriented and, towards the eastern sector of the Principal Cordillera, the structure is characterized by a series of east-verging thrusts repeating Mesozoic sequences in a typical thin-skinned fold-and-thrust belt: the Aconcagua fold-and-thrust belt (Ramos *et al.* 1996; Giambiagi & Ramos 2002; Giambiagi *et al.* 2003*a*, *b*; Armijo *et al.* 2010; Farías *et al.* 2010). This belt would have been active since *c.* 20 Ma

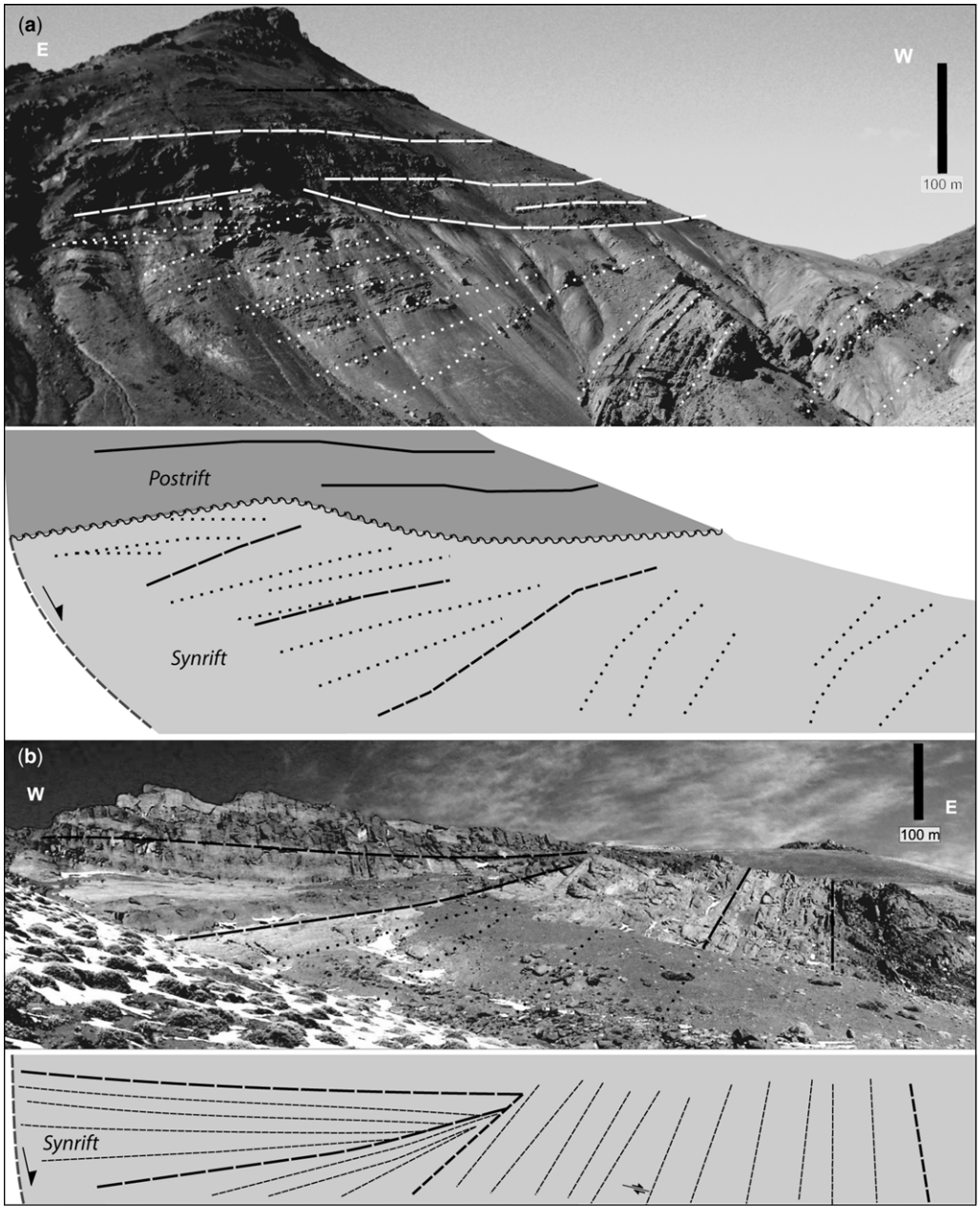

Fig. 12. Normal faulting affecting: (**a**) Early Miocene deposits at Las Llaretas; (**b**) the Cuartitos Unit at Tres Quebradas Creek.

(Cegarra & Ramos 1996). The early stages of deformation in this belt would be characterized by the inversion of Jurassic graben prior to the deposition of the volcanic levels of the Farellones Formation and then reactivated in the Late Miocene where migration of deformation to the east would have allowed the development of the Frontal Cordillera (Cegarra & Ramos 1996). As in the north (at the La Ramada fold-and-thrust belt), there is evidence of old normal faults inversion, but here these structures do not involve the basement significantly (Cegarra & Ramos 1996). Furthermore, like the

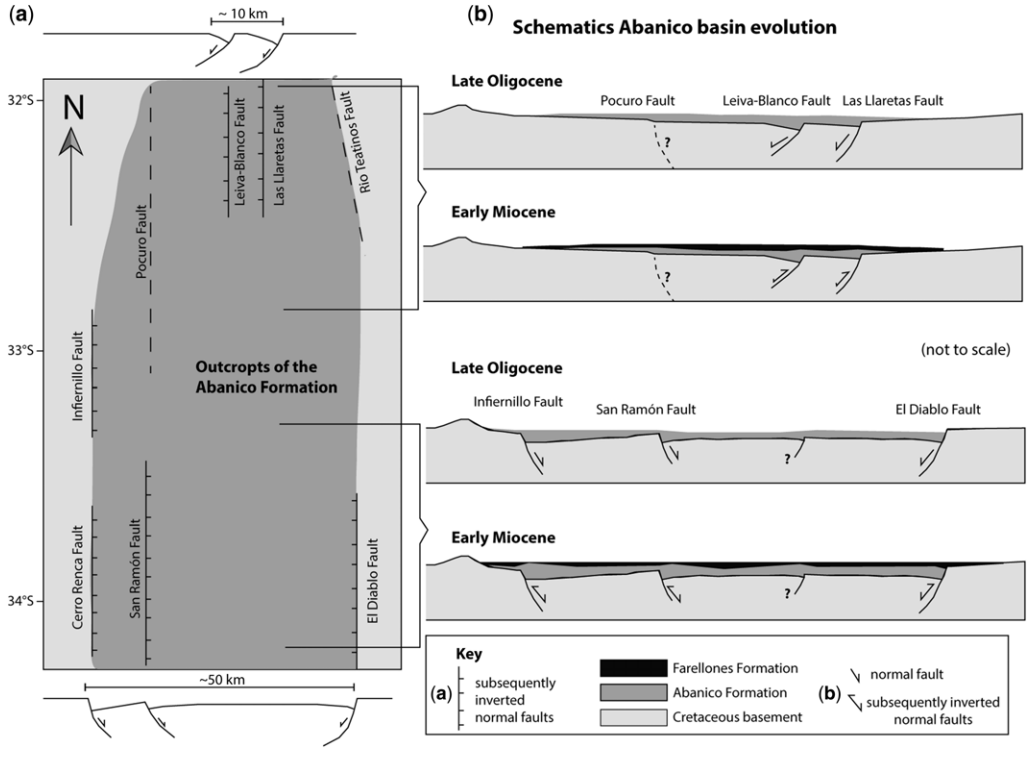

Fig. 13. (**a**) Schematic Abanico Formation outcrops and major structures that limit them in the Principal Cordillera between *c.* 32° and 34°S. We interprete the width of the basin where the deposits of the Abanico Formation accumulated. (**b**) Schematic of the Abanico Basin evolution between the Late Oligocene and Early Miocene at two generalized sections between 32°–33°S and 33°–34°S.

area of the La Ramada fold-and-thrust belt, the Chilean sector of the Principal Cordillera would have been affected by out-of-sequence thrusting, the development of which is not well constrained chronologically due to the structural complexity and scarcity of radiometric dating of some levels, so it is uncertain whether the out-of-sequence thrusts occurred before or after 8.6 Ma (Ramos *et al.* 1996).

For comparison purposes, we will focus on the strike of major structures and the width of the deformation zones. Our Type I model may explain in part the NNW orientation of compressive structures north of 33°S (Fig. 11), because the NNW-oriented out-of-sequence structures of the La Ramada fold-and-thrust belt, affecting the Abanico and Farellones formations in the eastern sector of the Principal Cordillera between 32° and *c.* 32°30′S, do not involve the basement and also do not correspond to a preferential orientation of the inverted normal faults that controlled the Abanico Basin (Fig. 13). The model shows that NNW-trending structures are generated in the region of lower basin width (northern zone), because when the same amount of shortening is induced throughout the region, the structures have an oblique orientation to accommodate more uplift in the north with respect to minor uplift on a wider region in the south (Fig. 8), where the structures are generated mainly within the pre-existing basin.

Moreover, the Type II model produces oblique structures generated by a progressive rotation process during the compressional phase. Because at *c.* 32°–32°30′S the Abanico extensional basin structures present approximately north–south strike and 21 Ma synrift associated strata, and given that post-21 Ma deformation affects both Abanico and Farellones formations (post-18 Ma) with NNW-oriented structures, a rotation process for developing these NNW-trending structures is discarded, because the process would also have rotated previous 18 Ma structures, which is not observed.

South of 33°S, the 'El Diablo' fault (Figs 10c, 11 & 13), located on the eastern boundary of the Chilean territory Principal Cordillera, corresponds to the westernmost structure of the east-verging Aconcagua fold-and-thrust belt and the fault that

would have limited the basin to the east (Fock 2005; Fock *et al.* 2006; Farías 2007). The Aconcagua fold-and-thrust belt developed folds with approximately NNW–SSE-oriented axes and approximately north–south-oriented faults (Giambiagi *et al.* 2003*a*, *b*). Some of these faults cut early developed folds and are therefore out-of-sequence faults. At this latitude, the eastern part of the Abanico Basin is deformed by backthrusts of the 'El Diablo' fault (Fock *et al.* 2006). The principal approximately north–south orientation of the 'El Diablo' fault and its associated backthrusts and the western part of the Aconcagua fold-and-thrust belt are consistent with the approximately north–south strike of the forethrusts and backthrusts that deformed the proximal-southern zone (wider basin zone) in the Type I model.

Based on evidence for the deposition of the Abanico Formation in a basin more than *c.* 50 km wide between 33° and 34°S (Fig. 13), controlled by normal faults (see Fock 2005), and the new data indicating that north of 33°S only distal deposits of this formation were accumulated in depocentres controlled by normal faults in a region *c.* 10 km wide (Jara & Charrier, in press), we believe that the Type I model might be representative of the palaeogeography existing between 32° and 34°S, where the space that accommodated clastic and volcaniclastic deposits is progressively narrower towards the north. Based on the above and on the results of the Type I model (Fig. 8), we can suggest that the curvature of the out-of-sequence faults of the La Ramada fold-and-thrust belt may be accounted for by a higher uplifting accommodation north of 33°S, compared to minor uplift accommodated in the larger width basin south of 33°S, regardless of or as a complement to the hypothesis that major inherited Pre-Andean normal structures would directly cause this oblique direction.

The evolution of the Type I model also allows us to make some interpretations. As deformation progresses, shortening in the southern zone is accommodated within the pre-existing basin, and the activity of the north–south elongated structures (Fig. 4b) is maintained throughout the process until the end of the compression. Instead, where shortening exceeds the amount of extension, the principal north–south structure (Fig. 4b) has less activity and has almost no activity in the centre of the model. If we make a comparison between the evolution of the main north–south elongated fault of the Type I model and our study area, we can illustrate this with the traces of the San Ramón and Pocuro fault zones (Fig. 10c), with the latter showing its main activity prior to the Early Miocene, deforming the Cretaceous outcrops intensely (Mpodozis *et al.* 2009; Jara & Charrier in press), with Miocene outcrops only slightly deformed. In fact, at 32°10′S latitude, west of the Pocuro Fault, almost flat-lying Oligocene–Miocene rocks cover unconformably deformed Cretaceous deposits of *c.* 82 Ma (Jara & Charrier, in press). In contrast, south of 33°S the San Ramón Fault shows evidence of important activity post-20 Ma (deforming the Abanico and Farellones formations' deposits) and even showing Quaternary activity (Rauld 2002; Armijo *et al.* 2008).

Further north, in the High Andes between 28°45′S and 30°30′S in the Norte Chico region of Chile, Early Oligocene to Late Miocene volcanic deposits have been designated as the Doña Ana Group (Martin *et al.* 1997), which consists of the Tilito (27–23 Ma) and Escabroso (21.5–17.5 Ma) formations (Maksaev *et al.* 1984; Mpodozis & Cornejo 1988; Kay *et al.* 1988, 1991; Bissig *et al.* 2001; Litvak 2009).

The older parts of the Doña Ana Group (Kay & Abbruzzi 1996) were probably deposited in an extensional basin subsequently inverted in Miocene times. The Doña Ana Group is partially coeval with the Abanico Formation further south (see Charrier *et al.* 2005, 2007). New studies show evidence of an extensional period in the Valle del Cura region located in the eastern Andean flank of the Pampean Flat Slab segment during the Oligocene. This corresponds to the intra-arc basin volcanic deposits of the Tilito Formation. This extensional basin affected the region between 29° and 30°S (Winocur 2010; Winocur & Ramos 2008, 2012; Winocur *et al.* 2014).

In this region, there is a series of sedimentary deposits of Jurassic age named the Lautaro Formation (Segerstrom 1959) and Cuartitos Unit (Martin *et al.* 1995), which are affected by normal faults formed in Late Triassic to Early Jurassic times (Winocur 2010). Some of these faults are preserved with a normal displacement recorded by a synsedimentary extensional structural setting (Fig. 12b). These normal structures, with mainly north–south strike, are almost completely preserved in this region after the Miocene compression. The structural cross-section (Fig. 14) shows the palinspastic restoration in Jurassic times at 29°30′S in the Norte Chico Region (Fig. 14c). Some of the normal faults that affected the Cuartitos Unit in Jurassic times are preserved in the structural cross-section (Fig. 14b). Some Jurassic normal faults were inverted in Miocene times, but there are also new faults created under compression in this period (Fig. 14b).

The north–south strike of normal structures preserved in the Type I model is consistent with the north–south orientation of normal faults of Jurassic age preserved in the 29°–30°S region (Winocur 2010). In the latter, it can be noted further that inverted Oligocene normal faults are concentrated

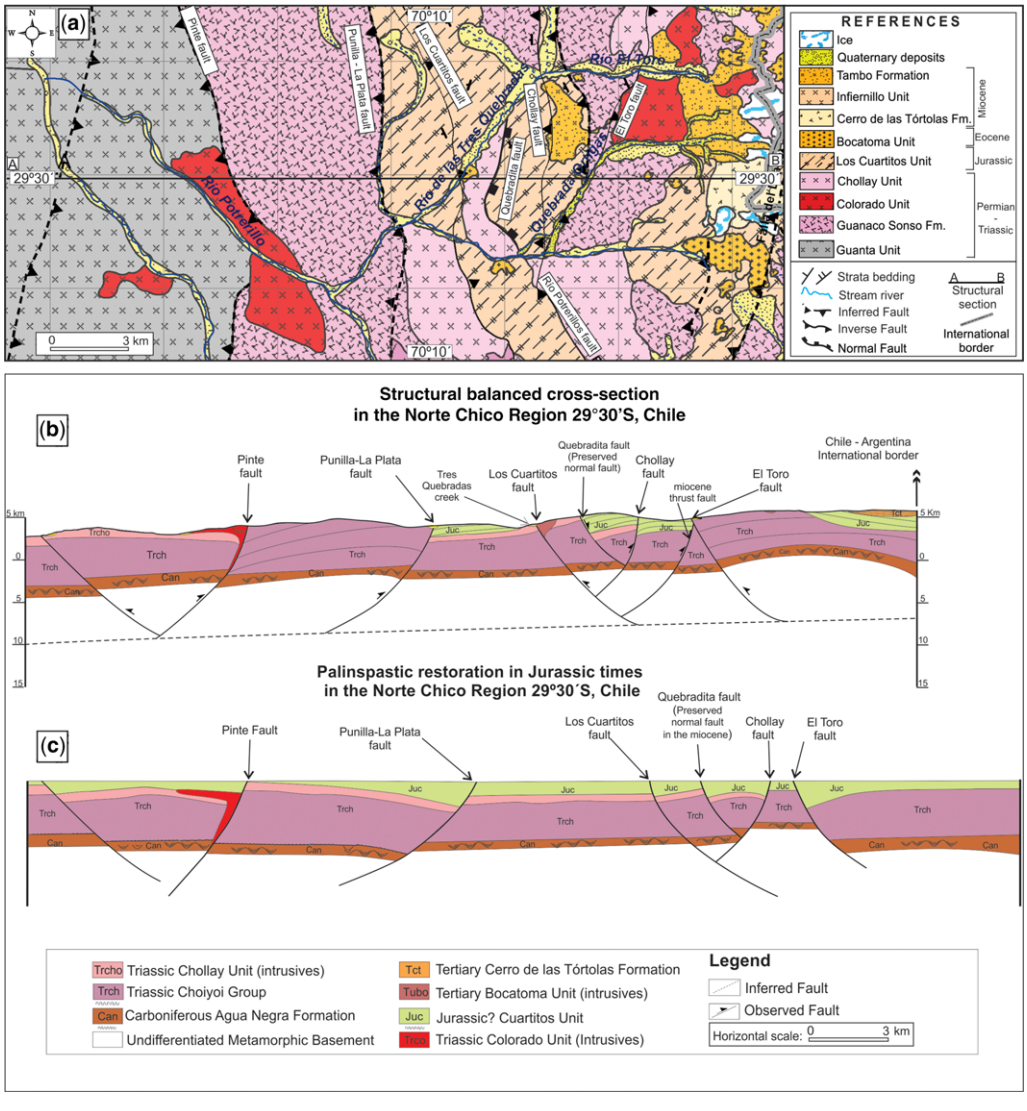

Fig. 14. (**a**) Geological map at *c.* 29°30′S. (**b**) Structural balanced cross-section. (**c**) Palinspastic restoration in the Norte Chico region, 29°30′S, Chile.

in the eastern region, with preserved Jurassic normal faults to the west (Winocur 2010), similar to what is observed in our and other analogue models (Bonini *et al.* 2012) where new inverse structures are concentrated near the mobile wall and inverted normal faults in the distal zone, away from the backstop.

Concluding remarks

The Type I model, reproducing differential extension and subsequent homogeneous compression, shows similar patterns to those of the natural field examples exposed here. In this model, compressive structures with uplift concentrated on a narrow area developed on the sector with smaller amounts of previous extension. In the region with greater extension, the compressive deformation was accommodated between the boundaries of the extensional basin, occupying a wider area, with consequent lower rising structures and topography. Furthermore, in the Type I model, these latitudinal differences of uplift between the northern and southern zones played an important role in the obliquity of

compressive structures. This is because, in the wider basin, zone shortening is concentrated within it, while to the north the structure turns its strike to accommodate more uplift close to the boundaries of the narrow basin.

Our Type I model shows that NNW-trending structures are generated in the region of smaller basin width (north), which is consistent with the orientantion of structures in the eastern sector of the Abanico Basin at *c.* 32°–33°S, where the NNW-oriented out-of-sequence structures of the La Ramada fold-and-thrust belt, affecting the Abanico and Farellones formations, do not involve the basement and do not correspond to a preferential orientation of the inverted normal faults that controlled the Abanico Basin.

The model shows that NNW-trending structures are generated in the narrower basin region to the north, which is consistent with a *c.* 10 km wide area of active depocentres during the Oligocene–Early Miocene at *c.* 32°10′S, in contrast to the region south of 33°S, where the basin would have been over 50 km wide. This result suggests that the curvature of the La Ramada fold-and-thrust belt may be influenced by a stronger and narrower uplifting north of 33°S compared to the smaller and wider uplift south of 33°S.

In the Type II model, with equal basin width and subsequent superimposed differential compression, the basin did not control the strike of the compressive structures. Conversely, regional structure is controlled by rotation during the shortening phase, which generates the greatest amount of folds and faults and greater uplift in the most compressed area. Thus, the Type II model can explain the development of oblique structures, but it needs an important oroclinal rotation, which is not consistent with geological observations of the studied region.

The experimental models developed show that the control exerted by the width of a pre-existing basin, which was subsequently reversed, has important implications in the resulting structural pattern and should be considered when interpreting the geological evolution of an inverted natural basin.

J. Likerman and E. O. Cristallini acknowledge funding from Laboratorio de Modelado Geológico (LaMoGe), Instituto de Estudios Andinos "Don Pablo Groeber" (IDEAN), Departamento de Ciencias Geológicas, FCEN, Universidad de Buenos Aires, C1428EGA, Argentina. D. Winocur and M. C. Ghiglione acknowledge funding from Laboratorio de Tectónica Andina, Instituto de Estudios Andinos "Don Pablo Groeber" (IDEAN), Departamento de Ciencias Geológicas, FCEN, Universidad de Buenos Aires, C1428EGA, Argentina. Funding for this project was provided by 'Ayuda para estadías cortas de investigación', Vicerrectoria de asuntos académicos, Departamento de postgrado y postítulo de la Universidad de Chile. We also acknowledge funding from Agencia de Promoción Científica, from Consejo Nacional de Investigaciones Científicas (CONICET, Argentina) and from LaMoGe (Universidad de Buenos Aires, UBA), and thank the colleagues and investigators working there for their generous contributions and valuable discussions regarding this research. The assistance of the Laboratorio de Modelamiento Analógico del Departamento de Geología de la Universidad de Chile, of the IGCP-586Y Unesco Proyect, and of L. Giambiagi (IANIGLA, Argentina) and L. Pinto (Universidad de Chile), for their collaboration in this contribution, is gratefully acknowledged. We also acknowledge the valuable ideas of T. Nalpas (Université de Rennes) and C. Jara (Universidad de Chile) in generating the experimental device and conducting the first test that led to the present study. This article is a contribution to FONDECYT Project 1120272: Extension, inversion and propagation: key tectonic styles on the development of the Andean Cordillera of Central Chile–Argentina (32°–36°S).

References

Agostini, A., Bonini, M., Corti, G., Sani, F. & Mazzarini, F. 2011. Fault architecture in the Main Ethiopian Rift and comparison with experimental models: implications for rift evolution and Nubia–Somalia kinematics. *Earth and Planetary Science Letters*, **301**, 479–492, http://dx.doi.org/10.1016/j.epsl.2010.11.024

Aguirre, L. 1960. Geología de Los Andes de Chile Central. *Instituto de Investigaciones Geológicas*, **9**.

Alvarez, P. P., Benoit, S. & Ottone, E. G. 1995. Las Formaciones Rancho de Lata, Los Patillos y otras unidades mesozoicas de la Alta Cordillera Principal de San Juan. *Revista de la Asociación Geológica Argentina*, **50**, 123–142.

Amilibia, A., Sabat, F., McClay, K. R., Munoz, J., Roca, E. & Chong, G. 2008. The role of inherited tectono-sedimentary architecture in the development of the central Andean mountain belt: insights from the Cordillera de Domeyko. *Journal of Structural Geology*, **30**, 1520–1539, http://dx.doi.org/10.1016/j.jsg.2008.08.005

Armijo, R., Rauld, R., Thiele, R., Vargas, G., Campos, J., Lacassin, R. & Kausel, E. 2008. An Andean megathrust synthetic to subduction? The San Ramón fault and associated seismic hazard for Santiago (Chile). *In*: *4th Alexander von Humboldt International Conference*. Santiago de Chile, 164.

Armijo, R., Rauld, R., Thiele, R., Vargas, G., Campos, J., Lacassin, R. & Kausel, E. 2010. The West Andean Thrust, the San Ramón Fault, and the seismic hazard for Santiago, Chile. *Tectonics*, **29**, 1–34, http://dx.doi.org/10.1029/2008TC002427

Bissig, T., Clark, A. H., Lee, J. K. W. & Heather, K. B. 2001. The Cenozoic history of volcanism and hydrothermal alteration in the Central Andean flat-slab region: new $^{40}Ar-^{39}Ar$ constraints from the El Indio–Pascua Au (–Ag, Cu) Belt, 29°20′–30°30′ S. *International Geology Review*, **43**, 312–340, http://dx.doi.org/10.1080/00206810109465016

Bonini, M., Souriot, T., Boccaletti, M. & Brun, J. P. 1997. Successive orthogonal and oblique extension

episodes in a rift zone: laboratory experiments with application to the Ethiopian Rift. *Tectonics*, **16**, 347, http://dx.doi.org/10.1029/96TC03935

Bonini, M., Sani, F. & Antonielli, B. 2012. Basin inversion and contractional reactivation of inherited normal faults: a review based on previous and new experimental models. *Tectonophysics*, **522–523**, 55–88, http://dx.doi.org/10.1016/j.tecto.2011.11.014

Brun, J. P. & Tron, V. 1993. Development of the North Viking graben: inferences from laboratory modelling. *Sedimentary Geology*, **86**, 31–51, http://dx.doi.org/10.1016/0037–0738(93)90132-O

Brun, J. P. & Nalpas, T. 1996. Graben inversion in nature and experiments. *Tectonics*, **15**, 677–687, http://dx.doi.org/10.1029/95TC03853

Buchanan, P. G. & McClay, K. R. 1991. Sandbox experiments of inverted listric and planar fault systems. *Tectonophysics*, **188**, 97–115, http://dx.doi.org/10.1016/0040-1951(91)90317-L

Buchanan, P. G. & McClay, K. R. 1992. Experiments on basin inversion above reactivated domino faults. *Marine and Petroleum Geology*, **9**, 486–500, http://dx.doi.org/10.1016/0264-8172(92)90061-I

Burbank, D. W., Vergés, J., Muñoz, J.-A. & Bentham, P. 1992. Coeval hindward- and forward-imbricating thrusting in the south-central Pyrenees, Spain: timing and rates of shortening and deposition. *Geological Society of America Bulletin*, **104**, 3–17, http://dx.doi.org/10.1130/0016-7606(1992)104<0003:CHAFIT>2.3.CO;2

Calassou, S., Larroque, C. & Malavieille, J. 1993. Transfer zones of deformation in thrust wedges: an experimental study. *Tectonophysics*, **221**, 325–344, http://dx.doi.org/10.1016/0040-1951(93)90165-G

Carey, S. 1958. The tectonic approach to continental drift. *In*: *Continental Drift: A Symposium*. Geology Department, University of Tasmania, Hobart, Tasmania, 177–355.

Cegarra, M. & Ramos, V. A. 1996. La Faja Plegada y Corrida del Aconcagua. *In*: Ramos, V. A. (ed.) *Geología de la región del Aconcagua, provincias de San Juan y Mendoza*. Subsecretaría de Minería de la Nación, Dirección Nacional del Servicio Geológico, Buenos Aires, 387–422.

Charrier, R. 1973. Interruptions of spreading and the compressive tectonic phases of the meridional andes. *Earth and Planetary Science Letters*, **20**, 242–249, http://dx.doi.org/10.1016/0012-821X(73)90164-7

Charrier, R., Baeza, O. *et al*. 2002. Evidence for Cenozoic extensional basin development and tectonic inversion south of the flat-slab segment, southern Central Andes, Chile (33°–36° S.L.). *Journal of South American Earth Sciences*, **15**, 117–139, http://dx.doi.org/10.1016/S0895-9811(02)00009-3

Charrier, R., Bustamante, M. *et al*. 2005. The Abanico extensional basin: regional extension, chronology of tectonic inversion and relation to shallow seismic activity and Andean uplift. *Neues Jahrbuch für Geologie und Paläontologie Abh*, **236**, 43–77.

Charrier, R., Pinto, L. & Rodríguez, M. 2007. Tectonostratigraphic evolution of the Andean Orogen in Chile. *In*: Moreno, W. & Gibbons, T. (eds) *The Geology of Chile*. The Geological Society, London, Special Publications, 21–116.

Charrier, R., Farías, M. & Maksaev, V. 2009. Evolución tectónica, paleogeográfica y metalogénica durante el Cenozoico en los Andes de Chile norte y central e implicaciones para las regiones adyacentes de Bolivia y Argentina. *Revista de la Asociación Geológica Argentina*, **65**, 5–35.

Cooper, M. & Williams, G. D. 1989. *Inversion tectonics*. Geological Society, London, Special Publications, **42**, i–vi, http://dx.doi.org/10.1006/jare.1999.0574

Cooper, M. A., Williams, G. D. *et al*. 1989. Inversion tectonics – a discussion. *In*: Cooper, M. A. & Williams, G. D. (eds) *Inversion Tectonics*. Geological Society, London, Special Publications, **44**, 335–347.

Corrado, S., Di Bucci, D., Naso, G. & Faccenna, C. 1998. Influence of palaeogeography on thrust system geometries: an analogue modelling approach for the Abruzzi–Molise (Italy) case history. *Tectonophysics*, **296**, 437–453, http://dx.doi.org/10.1016/S0040-1951(98)00147-4

Corti, G. 2003. Transition from continental break-up to punctiform seafloor spreading: how fast, symmetric and magmatic. *Geophysical Research Letters*, **30**, 1–4, http://dx.doi.org/10.1029/2003GL017374

Cotton, J. T. & Koyi, H. A. 2000. Modeling of thrust fronts above ductile and frictional detachments: application to structures in the Salt Range and Potwar Plateau, Pakistan. *Geological Society of America Bulletin*, **112**, 351–363, http://dx.doi.org/10.1130/0016-7606(2000)112<351:MOTFAD>2.0.CO;2

Coward, M. P. 1994. Inversion tectonics. *In*: Hancock, P. L. (ed.) *Continental Deformation*. Pergamon Press, Oxford, 289–304.

Coward, M. P., Gillcrist, R. & Trudgill, B. 1991. Extensional structures and their tectonic inversion in the Western Alps. *In*: Roberts, A., Yielding, G. & Freeman, B. (eds) *The Geometry of Normal Faults*. Geological Society, London, Special Publication, **56**, 93–112.

Cristallini, E. O. 1996. La faja plegada y corrida de la Ramada. *In*: Ramos, V. A. (ed.) *Geología de la región del Aconcagua, provincias de San Juan y Mendoza*. Subsecretaría de Minería de la Nación, Dirección Nacional del Servicio Geológico, Buenos Aires, 349–385.

Cristallini, E. O. & Cangini, A. 1993. Estratigrafia y estructura de las nacientes del rio Volcfin, Alta Cordillera de San Juan. *In*: *XII Congreso Geológico Argentino*, Buenos Aires, 85–92.

Cristallini, E. O. & Ramos, V. A. 2000. Thick-skinned and thin-skinned thrusting in the La Ramada fold and thrust belt: crustal evolution of the High Andes of San Juan, Argentina (32° SL). *Tectonophysics*, **317**, 205–235, http://dx.doi.org/10.1016/S0040-1951(99)00276-0

Cristallini, E. O., Mosquera, A. & Ramos, V. A. 1994. Estructura de la Alta Cordillera de San Juan. *Revista de la Asociación Geológica Argentina*, **49**, 165–183.

Dauteuil, O. & Brun, J. P. 1996. Deformation partitioning in a slow spreading ridge undergoing oblique extension: Mohns Ridge, Norwegian Sea. *Tectonics*, **15**, 870, http://dx.doi.org/10.1029/95TC03682

Del Ventisette, C., Montanari, D., Sani, F. & Bonini, M. 2006. Basin inversion and fault reactivation in laboratory experiments. *Journal of Structural*

Geology, **28**, 2067–2083, http://dx.doi.org/10.1016/j.jsg.2006.07.012

Dubois, A., Odonne, F., Massonnat, G., Lebourg, T. & Fabre, R. 2002. Analogue modelling of fault reactivation: tectonic inversion and oblique remobilisation of grabens. *Journal of Structural Geology*, **24**, 1741–1752, http://dx.doi.org/10.1016/S0191-8141(01)00129-8

Elliott, D. 1976. The motion of thrust sheets. *Journal of Geophysical Research*, **81**, 949, http://dx.doi.org/10.1029/JB081i005p00949

Faccenna, C., Nalpas, T., Brun, J. P., Davy, P. & Bosi, V. 1995. The influence of pre-existing thrust faults on normal fault geometry in nature and in experiments. *Journal of Structural Geology*, **17**, 1139–1149, http://dx.doi.org/10.1016/0191-8141(95)00008-2

Farías, M. 2007. *Tectónica y erosión en la evolución del relieve de los Andes de Chile Central durante el Neogeno*. PhD Thesis, Universidad de Chile, Santiago.

Farías, M., Comte, D. *et al.* 2010. Crustal-scale structural architecture in central Chile based on seismicity and surface geology: implications for Andean mountain building. *Tectonics*, **29**, TC3006, http://dx.doi.org/10.1029/2009TC002480

Fock, A. 2005. *Cronología y tectónica de la exhumación en el Neógeno de los Andes de Chile central entre los 33° y los 34°S*. MSc (unpublished), Departamento de Geología, Universidad de Chile, Santiago.

Fock, A., Charrier, R., Farías, M., Maksaev, V., Fanning, C. M. & Alvarez, R. 2005. Deformation and uplift of the western Main Cordillera between 33° and 34°S. *In*: *Proceedings 6th International Symposium on Andean Geodynamics (ISAG)*, Barcelona, Editions IRD (Institut de recherche pour le développement), 273–276.

Fock, A., Charrier, R., Maksaev, V. & Farias, M. 2006. Neogene exhumation and uplift of the Andean Main Cordillera from apatite fission tracks between 33°30′ and 34°00′ S. *In*: Mendoza, (ed.) *Backbone of the Americas – Patagonia to Alaska. Geological Society of America Meeting*, Mendoza, 102.

Gartrell, A., Hudson, C. & Evans, B. 2005. The influence of basement faults during extension and oblique inversion of the Makassar Straits rift system: insights from analog models. *American Association of Petroleum Geologists Bulletin*, **89**, 495–506, http://dx.doi.org/10.1306/12010404018

Ghiglione, M. C. & Cristallini, E. O. 2007. Have the southernmost Andes been curved since Late Cretaceous time? An analog test for the Patagonian Orocline. *Geology*, **35**, 13, http://dx.doi.org/10.1130/G22770A.1

Giambiagi, L. B. & Ramos, V. A. 2002. Structural evolution of the Andes in a transitional zone between flat and normal subduction (33°30′–33°45′S), Argentina and Chile. *Journal of South American Earth Sciences*, **15**, 101–116, http://dx.doi.org/10.1016/S0895-9811(02)00008-1

Giambiagi, L. B., Alvarez, P. P., Godoy, E. & Ramos, V. A. 2003*a*. The control of pre-existing extensional structures on the evolution of the southern sector of the Aconcagua fold and thrust belt, southern Andes. *Tectonophysics*, **369**, 1–19, http://dx.doi.org/10.1016/S0040-1951(03)00171-9

Giambiagi, L. B., Ramos, V. A., Godoy, E., Alvarez, P. P. & Orts, S. 2003*b*. Cenozoic deformation and tectonic style of the Andes, between 33° and 34° south latitude. *Tectonics*, **22**, http://dx.doi.org/10.1029/2001TC001354

Giambiagi, L. B., Alvarez, P. P., Bechis, F. & Tunik, M. A. 2005. Influencia de las estructuras de rift triásico-jurásicas sobre el estilo de deformación en las fajas plegadas y corridas de Aconcagua y Malargüe, Mendoza. *Revista de la Asociación Geológica Argentina*, **60**, 662–671.

Giambiagi, L. B., Ghiglione, M., Cristallini, E. O. & Bottesi, G. 2009*a*. Kinematic models of basement/cover interaction: insights from the Malargüe fold and thrust belt, Mendoza, Argentina. *Journal of Structural Geology*, **31**, 1443–1457, http://dx.doi.org/10.1016/j.jsg.2009.10.006

Giambiagi, L., Ghiglione, M. C., Cristallini, E. O. & Bottesi, G. 2009*b*. Características estructurales del sector sur de la faja plegada y corrida de Malargüe (35°–36°s): distribución del acortamiento e influencia de estructuras previas. *Revista de la Asociación Geológica Argentina*, **65**, 140–153.

Gillcrist, R., Coward, M. P., Trudgill, B., Pecher, A. & Mugnier, J. L. 1989. Structural inversion in the external French Alps. *In*: Cooper, M. A. & Williams, G. D. (eds) *Inversion Tectonics*. Geological Society, London, Special Publications, **44**, 354–354.

Godoy, E. 2011. Structural setting and diachronism in the Central Andean Eocene to Miocene volcano-tectonic basins. *In*: Salfity, J. A. & Marquillas, R. A. (eds) *Cenozoic Geology of the Central Andes of Argentina*. Instituto del Cenozoico, Universidad Nacional de Salta, Salta, 155–167.

Godoy, E. 2012. Sobre el variable marco geotectónico de las formarciones Abanico y Farellones y sus equivalentes al ser de los 35°LS. *Revista de la Asociación Geológica Argentina*, **69**, 570–577.

González, O. & Vergara, M. 1962. *Reconocimiento Geológico de la cordillera de los Andes entre los paralelos 35° y 38°S*. Universidad de Chile, Instituto de Geología Publicacion **24**.

Hubbert, M. K. 1937. Theory of scaled models as applied to the study of geological structures. *Geological Society of America Bulletin*, **48**, 1459–1519.

Hubbert, M. K. 1951. The mechanical basis for certain familiar geologic structures. *Geological Society of America Bulletin*, **62**, 355.

Huyghe, P. & Mugnier, J.-L. 1992. The influence of depth on reactivation in normal faulting. *Journal of Structural Geology*, **14**, 991–998, http://dx.doi.org/10.1016/0191-8141(92)90030-Z

Jackson, J. & McKenzie, D. 1983. The geometrical evolution of normal fault systems. *Journal of Structural Geology*, **5**, 471–482, http://dx.doi.org/10.1016/0191-8141(83)90053-6

Jara, P. & Charrier, R. In press. Nuevos antecedentes geocronológicos y estratigráficos para el Cenozoico de la Cordillera Principal de Chile entre 32° y 32°30′ S. Implicancias paleogeográficas y estructurales. *Andean Geology*. Online.

Jara, P., Piquer, J., Pinto, L. & Arriagada, C. 2009. Perfiles estructurales de la Cordillera Principal de

Chile Central: resultados preliminares. *In*: *Congreso Geológico Chileno*, Santiago, no. 12, S9–038.

KAY, S. M. & ABBRUZZI, J. M. 1996. Magmatic evidence for Neogene lithospheric evolution of the central Andean 'flat-slab' between 30°S and 32°S. *Tectonophysics*, **259**, 15–28, http://dx.doi.org/10.1016/0040-1951(96)00032-7

KAY, S. M., MAKSAEV, V., MOSCOSO, R., MPODOZIS, C., NASI, C. & GORDILLO, C. E. 1988. Tertiary Andean magmatism in Chile and Argentina between 28°S and 33°S: correlation of magmatic chemistry with a changing Benioff zone. *Journal of South American Earth Sciences*, **1**, 21–38, http://dx.doi.org/10.1016/0895-9811(88)90013-2

KAY, S. M., MPODOZIS, C., RAMOS, V. A. & MUNIZAGA, F. 1991. Magma source variations for mid–late Tertiary magmatic rocks associated with a shallowing subduction zone and a thickening crust in the central Andes (28 to 33 S). *In*: HARMON, R. S. & RAPELA, C. W. (eds) *Andean Magmatism and its Tectonic Setting*. Geological Society of America, Boulder, 113–138, http://dx.doi.org/10.1130/SPE265-p113

KELLER, J. V. A. & MCCLAY, K. R. 1995. *3D sandbox models of positive inversion*. *In*: BUCHANAN, J. G. B. & BUCHANAN, P. G. (eds) *Basin Inversion*. Geological Society, London, Special Publications, **88**. 137–146.

KLOHN, C. 1960. Geología de la Cordillera de los Andes de Chile Central, provincias de Santiago, O'Higgins, Colchagua y Curicó. *Instituto de Investigaciones Geológicas*, **8**, 95.

KNOTT, S. D., BEACH, A., WELBON, A. I. & BROCKBANK, P. J. 1995. Basin inversion in the Gulf of Suez: implications for exploration and development in failed rifts. *In*: BUCHANAN, J. G. B. & BUCHANAN, P. G. (eds) *Basin Inversion*. Geological Society, London, Special Publications, **88**, 59–81.

KONSTANTINOVSKAYA, E. A., HARRIS, L. B., POULIN, J. & IVANOV, G. M. 2007. Transfer zones and fault reactivation in inverted rift basins: insights from physical modelling. *Tectonophysics*, **441**, 1–26, http://dx.doi.org/10.1016/j.tecto.2007.06.002

KOOPMAN, A., SPEKSNIJDER, A. & HORSFIELD, W. T. 1987. Sandbox model studies of inversion tectonics. *Tectonophysics*, **137**, 379–388, http://dx.doi.org/10.1016/0040-1951(87)90329-5

KRANTZ, R. W. 1991. Measurement of friction coefficients and cohesion for faulting and fault reactivation in laboratory models using sand and sand mixtures. *In*: COBBOLD, P. R. (ed.) *Experimental and Numerical Modelling of Continental Deformation*. Tectonophysics, **188**, 203–207.

LIKERMAN, J., BURLANDO, J. F., CRISTALLINI, E. O. & GHIGLIONE, M. C. 2013. Along-strike structural variations in the Southern Patagonian Andes: insights from physical modeling. *Tectonophysics*, **590**, 106–120, http://dx.doi.org/10.1016/j.tecto.2013.01.018

LITVAK, V. D. 2009. El volcanismo Oligoceno superior–Mioceno inferior del Grupo Doña Ana en la Alta Cordillera de San Juan. *Revista de la Asociación Geológica Argentina*, **64**, 201–213.

MACEDA, R. & FIGUEROA, D. 1995. Inversion of the Mesozoic Neuquén Rift in the Malargüe fold and thrust belt, Mendoza, Argentina. *In*: TANKARD, A., SUAREZ, R. & WELSINK, H. (eds) *Petroleum Basins of South America*. American Association of Petroleum Geologists, **62**, 369–382.

MACEDO, J. & MARSHAK, S. 1999. Controls on the geometry of fold–thrust belt salients. *Geological Society of America Bulletin*, **111**, 1808–1822, http://dx.doi.org/10.1130/0016-7606(1999)111<1808:COTGOF>2.3.CO;2

MAKSAEV, V., MOSCOSO, R., MPODOZIS, C. & NASI, C. 1984. Las unidades volcánicas y plutónicas del Cenozoico superior en la alta cordillera del Norte Chico (29°–31° S): geología, alteración hidrotermal y mineralización. *Revista Geológica de Chile*, **21**, 11–51.

MANDAL, N. & CHATTOPADHYAY, A. 1995. Modes of reverse reactivation of domino-type normal faults: experimental and theoretical approach. *Journal of Structural Geology*, **17**, 1151–1163, http://dx.doi.org/10.1016/0191-8141(95)00015-6

MARSHAK, S. 2004. Salients, recesses, arcs, oroclines, and syntaxes – a review of ideas concerning the formation of map-view curves in fold–thrust belts. *In*: MCCLAY, K. R. (ed.) *Thrust Tectonics and Hydrocarbon Systems*. American Association of Petroleum Geologists, Memoirs, **82**, 131–156.

MARTIN, M., CLAVERO, J., MPODOZIS, C. & CUITIÑO, L. 1995. *Estudio geológico de la Franja El Indio, Cordillera de Coquimbo*. Servicio Nacional de Geología y Minería, Santiago, Informe Registrado IR-95-6, **1**, 1–238.

MARTIN, M., KATO, T. & CAMPOS, A. 1997. Stratigraphic, structural, metamorphic and timing constraints for the assembly of late Palaeozoic to Triassic rocks in the lake-district, Chile (40 S). *Proceedings VIII Congreso Geológico Chileno*, Antofagasta, 154–158.

MCCLAY, K. R. 1989. Analogue models of inversion tectonics. *In*: COOPER, M. A. & WILLIAMS, G. D. (eds) *Inversion Tectonics*. Geological Society, London, Special Publications, **44**, 41–59.

MCCLAY, K. & BUCHANAN, P. G. 1992. Thrust faults in inverted extensional basins. *In*: MCCLAY, K. R. (ed.) *Thrust Tectonics*. Chapman and Hall, London, 93–104.

MCCLAY, K. R., INSLEY, M. W. & ANDERTON, R. 1989. Inversion of the Kechika Trough, Northeastern British Columbia, Canada. *In*: COOPER, M. A. & WILLIAMS, G. D. (eds) *Inversion Tectonics*. Geological Society, London, Special Publications, **44**, 235–257.

MITRA, S. 1993. Geometry and kinematic evolution of inversion structures. *American Association of Petroleum Geologists Bulletin*, **77**, 1159–1191.

MITRA, S. & ISLAM, Q. 1994. Experimental (clay) models of inversion structures. *Tectonophysics*, **230**, 211–222, http://dx.doi.org/10.1016/0040-1951(94)90136-8

MOSQUERA, A. 1990. *Estudio geológico del extremo sur de la cordillera del Medio y Valle del río Mercedario, provincia de San Juan*. MSc (unpublished), Universidad de Buenos Aires, Departamento de Geología, Buenos Aires.

MPODOZIS, C. & CORNEJO, P. 1988. *Hoja Pisco Elqui, Región de Coquimbo, scale 1 : 250000*. Servicio Nacional de Geología y Minería, Chile.

MPODOZIS, C., BROCKWAY, H., MARQUARDT, C. & PERELLÓ, J. 2009. Geocronología U/Pb y tectónica de la región Los Pelambres-Cerro Mercedario: implicancias para la evolución cenozoica de los Andes del

centro de Chile y Argentina. *In*: *XII Congreso Geológico Chileno*, Santiago de Chile.

Muñoz, C., Pinto, L., Charrier, R. & Nalpas, T. In press. Miocene Abanico Basin inversion, Central Chile (33°–35°S): the importance of volcanic load and shortcut faults. *Andean Geology*.

Nalpas, T. & Brun, J. P. 1993. Salt flow and diapirism related to extension at crustal scale. *Tectonophysics*, **228**, 349–362, http://dx.doi.org/10.1016/0040-1951(93)90348-N

Nalpas, T., Le Douaran, S., Brun, J. P., Unternehr, P. & Richert, J. P. 1995. Inversion of the broad Fourteens Basin (offshore Netherlands), a small-scale model investigation. *Sedimentary Geology*, **95**, 237–250, http://dx.doi.org/10.1016/0037-0738(94)00113-9

Panien, M., Schreurs, G. & Pfiffner, A. 2005. Sandbox experiments on basin inversion: testing the influence of basin orientation and basin fill. *Journal of Structural Geology*, **27**, 433–445, http://dx.doi.org/10.1016/j.jsg.2004.11.001

Pérez, D. J. 1995. *Estudio geológico del cordón del Espinacito y regiones adyacentes, provincia de San Juan*. PhD thesis, Universidad de Buenos Aires.

Pérez, D. J. 1996. Los depósitos sinorogénicos. *In*: Ramos, V. A. (ed.) *Geología de la región del Aconcagua, provincias de San Juan y Mendoza*. Subsecretaría de Minería de la Nación, Dirección Nacional del Servicio Geológico, Buenos Aires, 317–341.

Pinto, L., Muñoz, C., Nalpas, T. & Charrier, R. 2010. Role of sedimentation during basin inversion in analogue modelling. *Journal of Structural Geology*, **32**, 554–565, http://dx.doi.org/10.1016/j.jsg.2010.03.001

Ramberg, H. 1981. *Gravity, Deformation and the Earth's Crust: In Theory, Experiments and Geological Application*. Academic Press, London/New York.

Ramos, V. A. 2006. Overview of the tectonic evolution of the southern Central Andes of Mendoza and Neuquén (35°–39° S latitude). *In*: Kay, S. M. & Ramos, V. A. (eds) *Evolution of an Andean Margin: A Tectonic and Magmatic View from the Andes to the Neuquén Basin (35°–39°S latitude)*. Geological Society of America, USA, Special Papers, 1–17, http://dx.doi.org/10.1130/2006.2407

Ramos, V. A., Cegarra, M. & Cristallini, E. O. 1996. Cenozoic tectonics of the high Andes of west–central Argentina (30–36 S latitude). *Tectonophysics*, **259**, 185–200.

Ranalli, G. 2000. Rheology of the crust and its role in tectonic reactivation. *Journal of Geodynamics*, **30**, 3–15, http://dx.doi.org/10.1016/S0264-3707(99)00024-1

Rauld, R. 2002. *Análisis morfoestructural del frente cordillerano: Santiago oriente entre el río Mapocho y Quebrada de Macul*. Thesis, Departamento de Geología., Universidad de Chile, Santiago.

Rauld, R. 2011. *Deformación cortical y peligro sísmico asociado a la falla San Ramón en el frente cordillerano de Santiago, Chile Central (33°S). PhD thesis*, Universidad de Chile, Santiago.

Reiter, K., Kukowski, N. & Ratschbacher, L. 2011. The interaction of two indenters in analogue experiments and implications for curved fold-and-thrust belts. *Earth and Planetary Science Letters*, **302**, 132–146, http://dx.doi.org/10.1016/j.epsl.2010.12.002

Rivera, O. & Yañez, G. 2007. Geotectonic evolution of the central Chile Oligo-Miocene volcanic arc, 33–34°S: Towards a multidisciplinary re-interpretation of the inherited lithospheric structures. *In*: *GeoSur*, *Abstracts*. GeoSur, Santiago, Chile, 138.

Sandiford, M., Hansen, D. L. & McLaren, S. N. 2006. Lower crustal rheological expression in inverted basins. *In*: Buiter, S. & Schreurs, G. (eds) *Analogue and Numerical Modelling of Crustal Scale Processes*. Geological Society, London, Special Publications, **253**, 271–283.

Scisciani, V. 2009. Styles of positive inversion tectonics in the Central Apennines and in the Adriatic foreland: implications for the evolution of the Apennine chain (Italy). *Journal of Structural Geology*, **31**, 1276–1294, http://dx.doi.org/10.1016/j.jsg.2009.02.004

Segerstrom, K. 1959. *Cuadrángulo Los Loros: provincia de Atacama*. Instituto de Investigaciones Geológicas, Santiago, Carta 1, **33**.

Sibson, R. H. 1985. A note on fault reactivation. *Journal of Structural Geology*, **7**, 751–754, http://dx.doi.org/10.1016/0191-8141(85)90150-6

Soto, R., Casas, A. M., Storti, F. & Faccenna, C. 2002. Role of lateral thickness variations on the development of oblique structures at the western end of the South Pyrenean Central Unit. *Tectonophysics*, **350**, 215–235, http://dx.doi.org/10.1016/S0040-1951(02)00116-6

Soto, R., Casas-Sainz, A. M. & Pueyo, E. L. 2006. Along-strike variation of orogenic wedges associated with vertical axis rotations. *Journal of Geophysical Research*, **111**, B10402, http://dx.doi.org/10.1029/2005JB004201

Thiele, R. 1980. *Hoja Santiago. Región Metropolitana. Carta Geológica de Chile, scale 1:250.000*. Instituto de Investigaciones Geológicas, Santiago, **29**, 21.

Thomas, W. 1990. Controls on locations of transverse zones in thrust belts. *Ecologae Geologicae Helvetiae*, **83**, 727–744.

Turner, J. P. & Williams, G. 2004. Sedimentary basin inversion and intra-plate shortening. *Earth-Science Reviews*, **65**, 277–304, http://dx.doi.org/10.1016/j.earscirev.2003.10.002

Van Keken, P. E., Spiers, C. J., Van den Berg, A. P. & Muyzert, E. J. 1993. The effective viscosity of rocksalt: implementation of steady-state creep laws in numerical models of salt diapirism. *Tectonophysics*, **225**, 457–476, http://dx.doi.org/10.1016/0040-1951(93)90310-G

Vergara, M. & Drake, R. E. 1979. Eventos magmáticos–plutónicos en Los Andes de Chile Central. *In*: *II Congreso Geológico Chileno*. 2., Arica, 6-11 Agosto, F19–F30.

Vergés, J. & Muñoz, J. A. 1990. Thrust sequences in the southern central Pyrenees. *Bulletin de la Société Géologique de Franc*, **VI**, 265–271.

Weijermars, R. 1986. Finite strain of laminar flows can be visualized in SGM36-polymer. *Naturwissenschaften*, **73**, 33–34, http://dx.doi.org/10.1007/BF01168803

Weijermars, R. & Schmeling, H. 1986. Scaling of Newtonian and non-Newtonian fluid dynamics without inertia for quantitative modelling of rock flow due to gravity (including the concept of

rheological similarity). *Physics of the Earth and Planetary Interiors*, **43**, 316–330, http://dx.doi.org/10.1016/0031-9201(86)90021-X

WEIJERMARS, R., JACKSON, M. P. A. & VENDEVILLE, B. 1993. Rheological and tectonic modeling of salt provinces. *Tectonophysics*, **217**, 143–174, http://dx.doi.org/10.1016/0040-1951(93)90208-2

WINOCUR, D. 2010. *Geología y estructura del Valle del Cura y el sector central del Norte Chico, provincia de San Juan y IV Región de Coquimbo, Argentina y Chile*. PhD thesis, Universidad de Buenos Aires.

WINOCUR, D. & RAMOS, V. A. 2008. Geología y Estructura del sector norte de la Alta Cordillera de la provincia de San Juan. *In*: *XVII Congreso Geológico Argentino*, Jujuy, 166–167.

WINOCUR, D. & RAMOS, V. A. 2012. Oligocene extensional tectonics at the Main Andes, Valle del Cura Basin, San Juan Province, Argentina. *In*: *XIII Congreso Geológico Chileno*, Antofagasta, 253–255.

WINOCUR, D. A., LITVAK, V. Y. & RAMOS, V. A. 2014. Magmatic and tectonic evolution of the Oligocene Valle del Cura basin, main Andes of Argentina and Chile: evidence for generalized extension. *In*: SEPÚLVEDA, S., GIAMBIAGI, L. B., MOREIRAS, S. M., PINTO, L., TUNIK, M., HOKE, G. D. & FARÍAS, M. (eds) *Geodynamic Processes in the Andes of Central Chile and Argentina*, Geological Society, London, Special Publications, **399**. First published online February 17, 2014, http://dx.doi.org/10.1144/SP399.2

YAGUPSKY, D. L., CRISTALLINI, E. O., FANTIN, J., VALCARCE, G., BOTTESI, G. & VARADE, R. 2008. Oblique half-graben inversion of the Mesozoic Neuquén Rift in the Malargüe fold and thrust belt, Mendoza, Argentina: new insights from analogue models. *Journal of Structural Geology*, **30**, 839–853, http://dx.doi.org/10.1016/j.jsg.2008.03.007

YAMADA, Y. & MCCLAY, K. R. 2003. Application of geometric models to inverted listric fault systems in sandbox experiments. Paper 2: insights for possible along strike migration of material during 3D hanging wall deformation. *Journal of Structural Geology*, **25**, 1331–1336, http://dx.doi.org/10.1016/S0191-8141(02)00160-8

ZAPATA, T. R. 1990. *Estudio geológico de la cordillera Casa de Piedra y del cordón Valle Hermoso*. Unpublished, Master Thesis. Departamento de Geología, Universidad de Buenos Aires.